

Nucleon tensor form factors at large N_c

Nam-Yong Ghim,^{1,*} Ho-Yeon Won,^{2,†} June-Young Kim,^{3,‡} and Hyun-Chul Kim^{1,§}

¹*Department of Physics, Inha University, Incheon 22212, Republic of Korea*

²*CPHT, CNRS, École polytechnique, Institut Polytechnique de Paris, 91120 Palaiseau, France*

³*Theory Center, Jefferson Lab, Newport News, VA 23606, USA*

(Dated: January 22, 2025)

We investigate nucleon tensor form factors in the large- N_c limit. In this picture, the nucleon emerges as a state of the N_c valence quarks, which were bound by pion mean fields that were created by the presence of the valence quarks self-consistently. We find that the tensor charge ($g_T^{u-d} = 0.99$) and the anomalous tensor magnetic moment ($\kappa_T^{u+d} = 7.61$) are dominated by valence quarks, while the tensor quadrupole moment ($Q_T^{u-d} = -7.02$) shows significant sea quark effects. We examine how these quantities vary as the average size of the pion mean field is changed, showing interpolation between non-relativistic quark and Skyrme limits. We also observe that g_T^{u-d} and κ_T^{u+d} depend weakly on the pion mass. In contrast, Q_T^{u-d} exhibits strong enhancement near the chiral limit. The numerical results are in good agreement with available lattice QCD data and provide predictions for unmeasured quantities.

CONTENTS

I. Introduction	1
II. Tensor form factors	2
A. Three-dimensional Breit frame	3
B. Two-dimensional Drell-Yan-West frame	3
III. Effective chiral theory	4
A. Nucleon in the mean-field picture	5
B. Zero-mode quantization	6
C. Spin-flavor structure	6
D. Scaling behavior and relations	8
E. Tensor form factors in the mean-field picture	9
F. Discrete level contribution	10
G. Gradient expansion	11
IV. Numerical results	13
V. Discussion	14
A. Non-relativistic quark model vs. the Skyrme model	14
B. Pion mass dependence	16
C. t dependence	16
VI. Summary and extensions	16
Acknowledgments	18
A. 3D distributions of the tensor structure	18
B. Intermediate cutoff and extrapolation	18
References	19

I. INTRODUCTION

Understanding the nucleon structure has been a fundamental issue in hadronic physics well over decades. Generalized parton distributions (GPDs) have emerged as a crucial tool in examining nucleon structure within quantum chromodynamics (QCD) [1–5]. GPDs parametrize nucleon matrix elements of quark and gluon light-ray operators at non-zero momentum transfer, unifying the concepts of parton distributions functions (PDFs) and form factors. Chiral-even structures have extensively studied and well understood. The chiral-even GPDs can be extracted experimentally from deeply virtual Compton scattering and hard-exclusive vector meson production [1–8]. In contrast, chiral-odd structures cannot be measured through these processes, and alternative methods proposed [9–20] face significant challenges. Consequently, dynamical information on chiral-odd GPDs, primarily based on model-dependent studies [21–27], remains limited. Despite these experimental and theoretical challenges, understanding chiral-odd GPDs is as equally important as their chiral-even counterparts for a comprehensive mechanical interpretation of nucleon structure. In the leading twist, four chiral-odd GPDs quantify the distribution of transversely polarized quarks within the nucleon [28]. Form factors for the antisymmetry tensor operator can be interpreted as the first Mellin moments of chiral-odd GPDs and will provide a constraint on the chiral-odd GPDs/PDFs. These moments are potentially extractable from polarization observables in semi-inclusive deep-inelastic scattering and, in principle, from dilepton production in polarized proton-proton collisions [29–32]. However, these methods may result in substantial theoretical and experimental uncertainties [33–38]. Lattice QCD simulations have provided results for the lowest x -moment of chiral-odd GPDs [39–41]. Beyond these computational estimates and the aforementioned experimental approaches, current knowledge of tensor form factor properties remains limited.

* E-mail: Namyong.ghim@inha.edu

† E-mail: hoyeon.won@polytechnique.edu

‡ E-mail: jykim@jlab.org

§ E-mail: hchkim@inha.ac.kr

Spontaneous breakdown of chiral symmetry (SB χ S) in QCD can be realized by the topological fluctuations of gauge fields in the instanton vacuum; see Refs. [42, 43] for a review. Instantons, solutions to the Yang-Mills equation in singular gauge and Euclidean time, exhibit characteristic dimensions: average size $\bar{\rho} \approx 1/3$ fm and mean separation $\bar{R} \approx 1$ fm. Instantons generate localized quark zero modes with definite chirality. These modes are subsequently delocalized and undergo chirality flips when quarks propagate and interact consecutively with instantons and antiinstantons through the instanton medium. This process causes SB χ S. This picture introduces a small parameter called the instanton packing fraction that enables a systematic expansion for studying SB χ S and hadronic correlation functions. Effective dynamics at the scale \bar{R} can be constructed using $1/N_c$ expansion techniques, including saddle point approximation and bosonization. This approach yields a description of quarks with the dynamical mass $M \sim 0.3 - 0.4$ GeV coupled to a chiral pion field. Within this framework, the nucleon emerges as a self-consistent mean-field solution characterized by a classical pion field (soliton) and quarks occupying single-particle states [44]. This mean-field approach provides a specific realization of the general baryon picture in large- N_c QCD [45]. It represents an interpolation between quark model and chiral soliton [46] descriptions, encompassing both as limiting cases [47, 48]. The picture of an effective chiral theory for the nucleon has been successfully applied to describing various hadronic observables; see Ref. [49] for a review.

In this paper, we employ an effective chiral theory in the large N_c limit to investigate the nucleon matrix element of the local antisymmetric tensor current, based on a previously described framework that preserves important QCD properties, such as sum rules and polynomial properties, for chiral-odd GPDs [50]. In addition, this approach [50] has provided valuable insights into the nucleon's spin-flavor structure for the matrix element of the chiral-odd partonic operator. In this work, we present numerical estimations of tensor form factors, systematically expanding in terms of the multipole order. Unlike previous studies [51–53], the current analysis is confined to the strict large N_c limit of QCD, ensuring consistency between chiral-odd GPDs [50] and tensor form factors. We will first revisit the tensor monopole (g_T) and tensor dipole (κ_T) form factors, offering more transparent insights into their dynamical information and correcting previous calculations of the tensor dipole form factors. We also explore the previously uninvestigated quadrupole structure of the tensor form factors ($\sim Q_T$). In addition to the tensor charge g_T and tensor anomalous magnetic moment κ_T , the quadrupole moment Q_T is equally important, which is also related to the leading-twist chiral-odd GPDs \tilde{H}_T . Then we examine the large- r behavior of the three-dimensional (3D) tensor distributions and investigates the pion mass dependence to elucidate the chiral properties of the tensor form factors. This comprehensive analysis provides a more complete and accu-

rate description of the nucleon tensor structure within the framework of the effective chiral theory.

The paper is organized as follows: Section II introduces the formalism for tensor form factors and we perform the multipole expansion in specific frames. Section III details the effective chiral theory and our calculation methods. Sections IV and V present our numerical results and discussion, respectively. Finally, we summarize our findings and offer concluding remarks in Section VI.

II. TENSOR FORM FACTORS

The nucleon matrix element of the local antisymmetric tensor operator is given by

$$\mathcal{M}^q[i\sigma^{\mu\nu}] = \langle N(p', s') | \bar{\psi}_q(0) i\sigma^{\mu\nu} \psi_q(0) | N(p, s) \rangle, \quad (1)$$

where ψ_q denotes the quark field operator with its flavor component $q = u, d, \dots$ and $\sigma^{\mu\nu} = \frac{i}{2}[\gamma^\mu, \gamma^\nu]$. The nucleon state is normalized to be $\langle N(p', s') | N(p, s) \rangle = (2\pi)^3 2p^0 \delta_{s's} \delta^{(3)}(\mathbf{p}' - \mathbf{p})$, where p' (p) denotes the final (initial) state momentum, and s' (s) represents the spin projection of the final (initial) nucleon state. Using the Lorentz covariance and discrete symmetries (time reversal, parity, hermiticity), the matrix element (1) is parameterized in terms of the three independent tensor form factors

$$\begin{aligned} \mathcal{M}^q[i\sigma^{\mu\nu}] = \bar{u} & \left[H_T^q i\sigma^{\mu\nu} + \tilde{H}_T^q \frac{P^\mu \Delta^\nu - \Delta^\mu P^\nu}{M_N^2} \right. \\ & \left. + E_T^q \frac{\gamma^\mu \Delta^\nu - \Delta^\mu \gamma^\nu}{2M_N} \right] u, \end{aligned} \quad (2)$$

where P and Δ denote respectively the average and difference of the momenta

$$P = \frac{p' + p}{2}, \quad \Delta = p' - p. \quad (3)$$

Note that the Dirac gamma matrices satisfy $\{\gamma^\mu, \gamma^\nu\} = 2g^{\mu\nu}$, and Dirac spinors are normalized to the nucleon mass $\bar{u}(p, s)u(p, s) = 2M_N$. In Eq. (2), the tensor form factors $H_T^q \equiv H_T^q(t; \mu)$, $\tilde{H}_T^q \equiv \tilde{H}_T^q(t; \mu)$, and $E_T^q \equiv E_T^q(t; \mu)$ are given as the real functions of the momentum transfer squared, $t = \Delta^2$, and can be understood as the first Mellin moments of the chiral-odd GPDs [54, 55]. Since the tensor current is not a conserved one, the form factors must essentially depend on the normalization scale μ . In this work we will suppress its dependence in the expressions, e.g., $H_T^q(t) := H_T^q(t; \mu)$.

The matrix element of the antisymmetric tensor operator can be analyzed in two distinct reference frames: the Drell-Yan-West frame and the 3D Breit frame. The two-dimensional (2D) Drell-Yan-West frame offers an unambiguous spatial interpretation of the form factor. On the other hand, the 3D Breit frame (BF) is hampered by an ambiguous spatial interpretation, because the wave

packets of the baryon states are not sufficiently localized. Thus, unless we treat the collective baryon system as non-relativistic, a proper interpretation of the 3D spatial distribution would be deviated by the relativistic corrections $\sim 20\%$ for the nucleon. However, in the large N_c limit of QCD, where the baryon mass M_B scales with $\sim N_c$, the baryon is almost static. Thus, we can reasonably consider the 3D Breit frame. This frame is particularly well suited for studying form factors from the perspective of the 3D partial wave expansion (multipole expansion). For a comprehensive understanding of tensor form factors, we need to examine both reference frames: the 3D BF for practical analysis in the large N_c limit, and the 2D Drell-Yan-West frame for clear interpretation. In the next section, we will conduct a multipole expansion of the matrix element given in Eq. (1) in both of these frames.

A. Three-dimensional Breit frame

Using the standard 3D BF, where $\mathbf{P} = \mathbf{0}$, we first study the tensor structure of the matrix elements. In this symmetric frame, P and Δ are given by

$$P = (P^0, \mathbf{0}), \quad \Delta = (0, \mathbf{\Delta}), \quad (4)$$

where the instant-form components are represented as $v = (v^0, \mathbf{v})$. Obviously, these momentum variables (4) satisfy the on-shell conditions

$$P \cdot \Delta = 0, \quad P^2 + \frac{\Delta^2}{4} = M_N^2. \quad (5)$$

The angular dependence of the 3D momenta (p, p') is only carried by the momentum transfer $\mathbf{\Delta}$. Therefore, the 3D multipole expansion of the matrix element (2) can be performed with respect to the momentum transfer $\mathbf{\Delta}$. The 3D rank- n irreducible tensors are defined by

$$\begin{aligned} Y_0 &= 1 & (L=0), \\ Y_1^i &= \frac{\Delta^i}{|\mathbf{\Delta}|} & (L=1), \\ Y_2^{ij} &= \frac{\Delta^i \Delta^j}{|\mathbf{\Delta}|^2} - \frac{1}{3} \delta^{ij} & (L=2), \end{aligned} \quad (6)$$

where i, j run over the 3D components $i, j = 1, 2, 3$. The angular momenta $(L = 0, 1, 2)$ of the irreducible tensors are indicated in Eq. (6). The matrix element of the nucleon depends not only on the momentum transfer, but also it is controlled by the spin polarizations s' and s of the initial and final nucleon states.

The spin structures appear as bilinear forms in the 2-component spinors χ describing the spin wave function of each nucleon in its rest frame,

$$\chi^\dagger(s') \hat{M} \chi(s). \quad (7)$$

In the following the quantization axis is chosen as the 3-axis, and the spinors χ are eigenspinors of the third component of the spin operator $\mathbf{S} = \boldsymbol{\sigma}/2$, where $\boldsymbol{\sigma}$ denotes the SU(2) Pauli matrix. Thus, the spin quantum numbers are given by the spin projection along the 3-axis in the rest frame,

$$s \equiv S_3, \quad s' \equiv S'_3. \quad (8)$$

The operator \hat{M} can be either a unit operator $\mathbf{1}$ or a component of the spin operator $\mathbf{S} = \boldsymbol{\sigma}/2$. In this context, the representations of the spin states in the 3D expansion are related to the orbital angular momentum L

$$\begin{aligned} \hat{M} &= \mathbf{1} & (L=0), \\ &= \sigma^i & (L=1). \end{aligned} \quad (9)$$

Using Eqs. (6) and (9), we perform the 3D multipole expansion of Eq. (2) for the separate 3D $0k$ - and ij -components:

$$\mathcal{M}^q[i\sigma^{0k}] = \mathbf{1} Y_1^i \sqrt{-t} \left[H_T^q + E_T^q + 2\tilde{H}_T^q \right], \quad (10a)$$

$$\begin{aligned} \mathcal{M}^q[i\sigma^{ij}] &= i\epsilon^{ijk} \sigma^k Y_0 2M_N \left[H_T^q + \frac{t}{6M_N^2} E_T^q \right] \\ &\quad - i\epsilon^{ijk} \sigma^m Y_2^{km} \frac{t}{2M_N} \left[\frac{1}{2} H_T^q + E_T^q \right]. \end{aligned} \quad (10b)$$

The canonical spin states, which are constructed by boosting the spin states at rest frame, are used in the multipole expansion of Eqs. (1) and (2). Here it is implied that the spin operators are contracted with the nucleon rest-frame spinors, and that the matrix element is given as a function of S_3 and S'_3 .

There are three independent multipole structures in Eqs. (10a) and (10b). These multipole structures can also be explained by addition of the orbital angular momentum. By combining Eqs. (6) and (9), and by considering parity and time-reversal symmetries, we can project the operators $i\sigma^{0k}$ and $i\sigma^{ij}$ in such a way that they contain the multipole structure of the orbital angular momentum $L = 1$. Note that this projection is consistent with Eq. (10). For example, the rank-2 tensor Y_2 ($L = 2$) contracted with the spin operator σ^i ($L = 1$) preserves the angular momentum of the operator $i\sigma^{ij}$ ($L = 1$). The parity of this structure is calibrated by the antisymmetric tensor ϵ^{ijk} , which is consistent with the second line of Eq. (10b); see Ref. [50] for details.

B. Two-dimensional Drell-Yan-West frame

We also examine the matrix element of the tensor operator using the standard two-dimensional (2D) Drell-Yan-West frame (DYWF), satisfying $\mathbf{P}_\perp = 0$. In this symmetric frame, P and Δ are given by

$$P = \left(P^+, \frac{4M_N^2 + |\mathbf{\Delta}_\perp|^2}{8P^+}, \mathbf{0}_\perp \right), \quad (11)$$

$$\Delta = (0, 0, \mathbf{\Delta}_\perp), \quad (12)$$

where the light-front components are represented as $v = (v^+, v^-, \mathbf{v}_\perp)$ and $v^\pm = (v^0 \pm v^3)/2$. Again, these momentum variables (12) satisfy the on-shell conditions (5). The angular dependence of the 2D momenta is carried only by the momentum transfer Δ_\perp . Therefore, the 2D multipole expansion of the matrix element (2) can be performed with respect to the momentum transfer Δ_\perp . The 2D irreducible rank- n tensors are defined by [56]

$$\begin{aligned} X_0 &= 1 & (L_3 = 0), \\ X_1^i &= \frac{\Delta_\perp^i}{|\Delta_\perp|} & (L_3 = \pm 1), \\ X_2^{ij} &= \frac{\Delta_\perp^i \Delta_\perp^j}{|\Delta_\perp|^2} - \frac{1}{2} \delta^{ij} & (L_3 = \pm 2), \end{aligned} \quad (13)$$

where i, j are the transverse components $i, j = 1, 2$. The longitudinal components of the orbital angular momentum ($L_3 = 0, \pm 1, \pm 2$) for the 2D irreducible tensors are indicated in Eq. (13). Similar to the 3D multipole expansion, the spin structure is represented by the 3D spin vector (9) with the rotational symmetry broken:

$$\begin{aligned} \mathbf{1} & & (L_3 = 0), \\ \sigma^3 & & (L_3 = 0), \\ \sigma^i & & (L_3 = \pm 1), \end{aligned} \quad (14)$$

where $i = 1, 2$. Using Eqs. (13) and (14), we perform the 2D multipole expansion of Eq. (2) for the $+j$ component:

$$\begin{aligned} \mathcal{M}^q[i\sigma^{+j}] &= 2P^+ \left[i\epsilon^{3jm} \sigma^m X_0 \left\{ H_T^q - \frac{t}{4M_N^2} \tilde{H}_T^q \right\} \right. \\ &\quad + \mathbf{1} X_1^j \frac{\sqrt{-t}}{2M_N} \left\{ E_T^q + 2\tilde{H}_T^q \right\} \\ &\quad \left. + i\epsilon^{3jl} \sigma^m X_2^{lm} \frac{t}{4M_N^2} \left\{ 2\tilde{H}_T^q \right\} \right]. \end{aligned} \quad (15)$$

Here, the light-front helicity states, which are constructed by performing the light-front boost on the spin states at rest, are used in the multipole expansion of Eq. (2). Similar to Eq. (10) the spin operators can also be contracted with the nucleon rest-frame spinors. The matrix element of the $+j$ -component of the tensor operator consists of the 2D monopole, dipole, and quadrupole structure, respectively,

$$\begin{aligned} &\left[H_T^q - \frac{t}{4M_N^2} \tilde{H}_T^q \right], \\ &\left[E_T^q + 2\tilde{H}_T^q \right], \\ &\left[2\tilde{H}_T^q \right]. \end{aligned} \quad (16)$$

In the forward limit, $t \rightarrow 0$, the tensor multipole form factors become respectively the tensor charge, the anomalous tensor magnetic moment, and the tensor quadrupole

moment:

$$\begin{aligned} H_T^q(0) &= g_T^q, \\ E_T^q(0) + 2\tilde{H}_T^q(0) &= \kappa_T^q, \\ 2\tilde{H}_T^q(0) &= Q_T^q. \end{aligned} \quad (17)$$

The number of the multipole structure (15) can also be explained by the addition of the longitudinal orbital angular momentum. At the leading twist accuracy, the orbital angular momentum ($L_3 = \pm 1$) of the chiral-odd operator can be formed by combining Eqs. (13) and (14) and by considering the discrete symmetries. The maximum rank of the orbital angular momentum can reach the quadrupole tensor X_2 ($L_3 = \pm 2$) combined with the spin dipole operator σ^i ($L_3 = \pm 1$). The parity of this multipole structure is controlled by the antisymmetric tensor ϵ^{ijk} . In this way the whole multipole structure in Eq. (15) can be explained; see Ref. [50] for details.

On the other hand, the orbital angular momentum of the chiral-even operator ($\gamma^+, \gamma^+ \gamma_5$) at the leading twist is $L_3 = 0$. Therefore, the quadrupole orbital angular momentum (X_2) cannot be constructed. The possible maximum multipole is the dipole orbital angular momentum X_1 ($L_3 = \pm 1$) coupled with the dipole spin σ^i ($L_3 = \pm 1$). This means that the quadrupole structure appears uniquely in the nucleon matrix element of the chiral-odd operator at the leading twist accuracy.

One of the virtues of the multipole expansion lies in the fact that we can easily understand the physical meaning of the form factors. The Fourier transform of the given multipole form factors (16) can be understood as the impact parameter distribution. The multipole form factors and the multipole pattern of the impact parameter distribution have one-to-one correspondence. For example, the dipole $E_T + 2\tilde{H}_T$ and quadrupole $2\tilde{H}_T$ form factors quantify how the transversely polarized quark distributions are distorted in the form of the dipole and quadrupole patterns in the impact parameter space; see Ref. [28] for details. Therefore, the new basis (16) has a clear physical interpretation and can be employed in discussion of the nucleon structure.

III. EFFECTIVE CHIRAL THEORY

The SB χ S in QCD is realized by the topological fluctuations of the gauge fields in the instanton vacuum. Based on this picture, effective dynamics [43, 44] at the scale \bar{R} has emerged at large N_c . This effective theory is characterized by the low-energy QCD partition function

$$Z_{\text{eff}} = \int \mathcal{D}U \exp(iS_{\text{eff}}), \quad (18)$$

where the effective chiral action is given by

$$\begin{aligned} \exp(iS_{\text{eff}}[U]) &= \int \mathcal{D}\psi \mathcal{D}\bar{\psi} \\ &\times \exp \left[\int d^4x \bar{\psi}(x) (i\cancel{\partial} - MU\gamma_5 - \hat{m}) \psi(x) \right]. \end{aligned} \quad (19)$$

\hat{m} represents the current quark mass. We assume isospin symmetry with $m_u = m_d = m$, so that the mass matrix is proportional to the unit matrix, i.e., $\hat{m} = \text{diag}(m, m)$. This picture describes quarks with the dynamical mass M (approximately 0.3–0.4 GeV) coupled to a chiral pion field $U\gamma_5$. While M generally depends on the momentum of the quark, $\bar{\rho}^{-1} \approx 0.6$ GeV serves as a natural ultraviolet (UV) cutoff in this theory. For simplicity, M is treated as a constant by introducing a UV cutoff $\Lambda \approx \bar{\rho}^{-1}$. The SU(2) chiral fields U are defined as:

$$\begin{aligned} U &= \exp\{i\pi^a(x)\tau^a\}, \\ U\gamma_5 &= \exp\{i\pi^a(x)\tau^a\gamma_5\} = \frac{1+\gamma_5}{2}U + \frac{1-\gamma_5}{2}U^\dagger, \end{aligned} \quad (20)$$

where $\pi^a(x)$ ($a = 1, 2, 3$) represents the pseudo-Nambu-Goldstone (pNG) boson field, and τ^a is the SU(2) flavor matrix. The low normalization point of this theoretical framework is about 600 MeV, which is the inverse of the average instanton size $\bar{\rho}^{-1}$ (see Ref. [57]).

A. Nucleon in the mean-field picture

The nucleon in this framework emerges as a self-consistent mean-field solution, characterized by the classical pion field and quarks in single-particle states. This mean-field solution is obtained by using semiclassical approximation, which is justified at large N_c . In this approach, developed by Diakonov et al. [44], the nucleon emerges as a state consisting of the N_c valence quarks bound by the pion mean field. In this section we will give a brief summary of this mean-field approach.

In Euclidean space, the correlation function of baryon currents composed of the N_c valence quark fields, are computed in the effective chiral theory (19) by employing the saddle point approximation (semiclassical approximation) which is valid at large N_c . The mean-field solution is characterized by a nontrivial classical chiral field U_{cl} , which is obtained by solving the saddle-point equation or the classical equation of motion:

$$\left. \frac{\delta S_{\text{eff}}[U]}{\delta U} \right|_{U=U_{\text{cl}}} = 0. \quad (21)$$

The solution is time-independent (static) of the Euclidean time and has a specific spatial configuration, where the isospin orientation aligns with the spatial direction, forming a structure known as a ‘‘hedgehog’’ [58]:

$$\begin{aligned} U_{\text{cl}}(\mathbf{x}) &= \exp\{i\pi_{\text{cl}}^a(\mathbf{x})\tau^a\}, \\ \pi_{\text{cl}}^a(\mathbf{x}) &= \frac{x^a}{|\mathbf{x}|}P(r), \quad (a = 1, 2, 3). \end{aligned} \quad (22)$$

$P(r)$ denotes a radial profile function with $P(0) = \pi$ and $P(\infty) = 0$, where $r \equiv |\mathbf{x}|$ represents the magnitude of the position vector. This field configuration maintains invariance under simultaneous spatial and flavor rotations, and thus embodies the emergent spin-flavor symmetry of baryons in the large- N_c limit.

The quark field can be represented in a first-quantized representation, where the quarks occupy the single-particle states within the classical chiral field. These states are governed by the one-body Dirac Hamiltonian

$$\begin{aligned} H(U_{\text{cl}}) &= -i\gamma^0\gamma^k\partial_k + \gamma^0MU_{\text{cl}}\gamma_5 + \gamma^0\hat{m}, \\ H\Phi_n(\mathbf{x}) &= E_n\Phi_n(\mathbf{x}) \end{aligned} \quad (23)$$

in Minkowski space. Because of the hedgehog structure mentioned above, the Hamiltonian commutes with the grand spin $\mathbf{G} = \mathbf{\Sigma}/2 + \mathbf{T} + \mathbf{L}$ and the parity operators $\hat{\Pi}$,

$$[H, \mathbf{G}] = 0, \quad [H, \hat{\Pi}] = 0, \quad (24)$$

where $\mathbf{\Sigma} = -\gamma_0\boldsymbol{\gamma}\gamma_5$, $\mathbf{T} = \boldsymbol{\tau}/2$, and $\mathbf{L} = \mathbf{x} \times \mathbf{p}$ denote the spin, isospin, and orbital angular momentum operators, respectively. The quark state is thus characterized by the corresponding quantum numbers:

$$\begin{aligned} |n\rangle &\equiv |n = \{E_n, G, G_3, \Pi\}\rangle, \\ \text{with } \Phi_n(\mathbf{x}) &\equiv \langle \mathbf{x} | n \rangle. \end{aligned} \quad (25)$$

The one-body Dirac Hamiltonian (23) is solved in the presence of the static pion field to determine the eigenfunctions $\Phi_n(\mathbf{x})$ and eigenenergies E_n of the massive quark. This diagonalization is carried out within a finite-sized box, employing the ‘‘finite box’’ method developed by Ripka and Kahana [59, 60] (see also Ref. [49] for a review). The energy spectrum of the system consists of a discrete level with energy $E_{\text{lev}} < M$ and spectra of continuum levels with energies $E_n < M$ and $E_n > M$. In the ground state of a nucleon with baryon number $B = 1$, both the discrete level and the negative continuum are occupied by N_c quarks.

The energy of the classical nucleon, to the leading order in the $1/N_c$ expansion, is derived by the sum of the energies of the discrete level and the negative continuum, with the vacuum energy subtracted:

$$\begin{aligned} M_N &= N_c \sum_{n, \text{occ}} E_n - \text{vac} \\ &= N_c E_{\text{lev}} + N_c \sum_{E_n < 0} E_n - \text{vac}, \end{aligned} \quad (26)$$

where ‘‘occ’’ encompasses both the discrete level and the negative continuum level. Since the resulting energy is logarithmically divergent, it is not sensitive to a specific regularization scheme. In this study, we use the proper-time regularization to tame the UV divergence of the Dirac continuum (see Ref. [49]).

B. Zero-mode quantization

As mentioned previously, $1/N_c$ mesonic quantum fluctuations have been neglected. So, the nucleon is still a classical one, which does not carry proper quantum numbers. The pion mean field has still quantum fluctuations arising from translational and rotational zero modes, which do not change the energy of the classical nucleon. Since these zero modes are related to rotational and translational symmetries, and are not at all small, we have to integrate over them completely. Then they furnish the classical nucleon with proper quantum numbers, we must integrate over the zero-mode fluctuations in a complete manner. For the detailed explanation about the zero modes within the framework of the pion mean-field approach, we refer to Refs. [44, 49, 61]. Here, we recapitulate briefly the zero-mode quantization within the present framework.

The zero-mode quantization is summarized in terms of the following functional integral over the pNG fields

$$\int \mathcal{D}U \mathcal{F}[U(\mathbf{x})] \rightarrow \int \mathcal{D}\mathbf{Z} \int \mathcal{D}R \mathcal{F}[TRU_{\text{cl}}(\mathbf{x})R^\dagger T^\dagger]. \quad (27)$$

The integration over U can be computed by the saddle-point approximation, which gives the pion mean-field solution. The integrations over T and R are those over the translational and rotational zero modes, respectively. They stand respectively for the translational and rotational transformations that reflect the three translational zero modes and three rotational ones. T denotes the displacement operator that provides the momentum with the nucleon, and R is the $SU(2)$ unitary matrix. T translates the mean field from \mathbf{x} to $\mathbf{x} - \mathbf{X}$. The functional $\mathcal{F}[U]$ is a generic expression for any correlation function in the presence of the mean field.

Having imposed the boundary conditions at infinite Euclidean time separation, we show that the Fourier transform naturally appears and the functional integral is reduced to that over the flavor rotation R . Note that the integral over the flavor rotations is normalized to unity $\int dR = 1$. The integration over R yields the collective Hamiltonian for a spherical top, which provides $1/N_c$ rotational corrections to the nucleon mass. The eigenfunctions of the Hamiltonian describe a baryon state with the quantization condition $S = T$, so that the lowest baryon state ($S = T = 1/2$) is the nucleon, and the next state from the rotational excitation ($S = T = 3/2$) is identified as the Δ isobar. The wave functions ϕ_B are just the $SU(2)$ Wigner function expressed as

$$\begin{aligned} \phi_B(R) &\equiv \phi_{S_3 T_3}^{S=T}(R) \\ &= (-1)^{T+T_3} \sqrt{2T+1} D_{-T_3 S_3}^{T=S}(R), \end{aligned} \quad (28)$$

where the baryon quantum numbers are given by

$$B = \{S = T, S_3, T_3\}. \quad (29)$$

Here, S and T denote the baryon spin and isospin quantum numbers, respectively, and S_3 and T_3 represent the corresponding third components.

Once the zero-mode quantization is performed, the matrix element of an effective QCD operator between the baryon states is expressed as

$$\begin{aligned} \langle B', \mathbf{p}' | \hat{O} | B, \mathbf{p} \rangle &= \int d^3 \mathbf{X} e^{i(\mathbf{p}' - \mathbf{p}) \cdot \mathbf{X}} \\ &\times \int dR \phi_{B'}^*(R) \dots \phi_B(R). \end{aligned} \quad (30)$$

The ellipsis in eq. (30) denotes a mean-field correlation function expressed in terms of the effective QCD operator (\hat{O}) given as functions of the collective coordinates (\mathbf{X}, R) . In addition, this correlation function depends on the configuration of the pion mean field (U_{cl}) and the one-particle wave functions and energies. The explicit expression of Eq. (30) will be presented in Section III C.

Since we aim at investigating the tensor form factors at large N_c , we want to remark on the normalization of the baryon states and the N_c scaling of kinematical variables. The masses of the lowest-lying baryons are of the order N_c , and their mass splitting is of the order $1/N_c$:

$$M_\Delta = M_N \times N_c^1, \quad M_\Delta - M_N \propto N_c^{-1}. \quad (31)$$

In the $1/N_c$ expansion of the matrix element of the baryon states (30), the 3-momentum and energies of the baryon states B' and B have the following N_c scalings:

$$\begin{aligned} |\mathbf{p}'|, |\mathbf{p}| &\propto N_c^0, \\ p'^0, p^0 &= M_N + \mathcal{O}(N_c^{-1}) \propto N_c^1. \end{aligned} \quad (32)$$

In this context, the baryon state in eq. (30) is normalized to

$$\begin{aligned} \langle B', \mathbf{p}' | B, \mathbf{p} \rangle &= 2M_N \delta_{B'B} (2\pi)^3 \delta^{(3)}(\mathbf{p}' - \mathbf{p}), \\ \delta_{B'B} &= \delta_{S'S} \delta_{T'T} \delta_{S_3'S_3} \delta_{T_3'T_3}. \end{aligned} \quad (33)$$

Note that both the center-of-mass coordinates $\mathbf{X}(t)$ and the rotation matrix $R(t)$ in Eq. (27) exhibit a weak time dependence. The gradual displacement and rotation of the soliton generate kinetic corrections, which are suppressed in the $1/N_c$ expansion. In this work, thus, we concentrate on the rotational and translational zero modes to the zeroth-order corrections, so-called strict large N_c .

C. Spin-flavor structure

We are now in a position to apply the local tensor operator,

$$\hat{O} = \bar{\psi}_q i \sigma^{\mu\nu} \psi_q, \quad (34)$$

to Eq. (30), and derive the spin-flavor structure for the matrix element of Eq. (34) in the pion mean-field approach. In Ref. [50] an abstract mean-field approach was taken and the spin-flavor structure for the matrix element of the non-local/local tensor operator was derived. Based on this, the N_c scalings of “mean-field” form factors and large- N_c relations were established. Indeed, we confirm that the spin-flavor structure obtained in the current approach is consistent with the results of Ref. [50].

In the mean-field picture, the matrix element of the effective local QCD operator (34) is written as

$$\mathcal{M}^q[i\sigma^{\mu\nu}] = \langle B', \mathbf{p}' | \bar{\psi}_q(0) i\sigma^{\mu\nu} \psi_q(0) | B, \mathbf{p} \rangle, \quad (35)$$

where the baryon state is normalized as given in Eq. (33) in the leading order of the $1/N_c$ expansion. After computing the three-point correlation function (35) in the mean-field picture, we obtain the matrix elements of the tensor operator (34) for both isoscalar and isovector components in terms of the first-quantized representation:

$$\begin{aligned} \left\{ \begin{array}{l} \mathcal{M}^{u+d}[i\sigma^{0k}] \\ \mathcal{M}^{u-d}[i\sigma^{ij}] \end{array} \right\} &= 2M_N N_c \left\{ \begin{array}{l} \langle \mathbf{1} \rangle_{B'B} \\ \langle D^{3k} \rangle_{B'B} \end{array} \right\} \\ &\times \sum_{n, \text{occ}} \langle n | \left\{ \begin{array}{l} \gamma^0 i\sigma^{0k} \\ \gamma^0 i\sigma^{ij} \end{array} \right\} e^{i\Delta \cdot \hat{\mathbf{X}}} | n \rangle \Big|_{\text{reg}}, \end{aligned} \quad (36)$$

The notation $\dots|_{\text{reg}}$ indicates that a specific regularization was considered. This procedure depends on the type of divergence of the matrix element. It will be explored in Sec. III G.

The integral over the flavor matrix R in Eq. (30) is regarded as the matrix element of the spin-flavor operator $O(R)$,

$$\langle O \rangle_{B'B} \equiv \int dR \phi_{B'}^*(R) O(R) \phi_B(R). \quad (37)$$

In the leading order of the $1/N_c$ expansion, two different types of the spin-flavor operators, i.e., $\mathbf{1}$ and D^{3a} , appear. The matrix elements of these operators are obtained to be

$$\begin{aligned} \langle \mathbf{1} \rangle_{B'B} &= \delta_{B'B}, \\ \langle D^{3a} \rangle_{B'B} &= -\sqrt{\frac{2S+1}{2S'+1}} \\ &\times \langle TT_3, 10 | T'T'_3 \rangle \langle SS_3, 1a | S'S'_3 \rangle. \end{aligned} \quad (38)$$

Here, $\langle TT_3, 10 | T'T'_3 \rangle$ and $\langle SS_3, 1a | S'S'_3 \rangle$ represent the Clebsch-Gordan coefficients. Depending on the choice of the quantum numbers of the initial and final states, one derive not only the $N \rightarrow N$ matrix element, but also $N \rightarrow \Delta$ and $\Delta \rightarrow \Delta$ matrix elements; see Ref. [62].

Equation (36) also includes an infinite tower of the partial waves $e^{i\Delta \cdot \hat{\mathbf{X}}}$ that comes from the translational zero mode, where $\hat{\mathbf{X}}$ represents the 3D displacement operator. This factor plays an essential role in the multipole

expansion in the mean-field picture. On the other hand, Eq. (36) is obviously independent of the average momentum \mathbf{P} , which is natural in the picture of the static mean field. Using Eq. (32), we find the N_c scalings of these average and difference between initial and final momenta:

$$\begin{aligned} P^0 &\propto N_c^1, & P^i &\propto N_c^0, \\ \Delta^0 &\propto N_c^{-1}, & \Delta^i &\propto N_c^0. \end{aligned} \quad (39)$$

These results imply that each partial wave generated by $e^{i\Delta \cdot \hat{\mathbf{X}}}$ in Eq. (36) has the same N_c scalings, and that the translational correction $\mathbf{P}/2M_N$ is suppressed in $1/N_c$ expansion.

In this context, the matrix element (36) depends only on Δ . Thus, by performing the multipole expansion in Eq. (36) in powers of Δ , we derive its spin-flavor structure for the isoscalar and isovector components, respectively

$$\mathcal{M}^{u+d}[i\sigma^{0k}] = Y_1^i \langle \mathbf{1} \rangle_{B'B} \sqrt{-t} F_{\text{mf},1}^{u+d}, \quad (40a)$$

$$\begin{aligned} \mathcal{M}^{u-d}[i\sigma^{ij}] &= -i\epsilon^{ijk} \langle D^{3k} \rangle_{B'B} Y_0^6 M_N F_{\text{mf},0}^{u-d} \\ &+ i\epsilon^{ijk} \langle D^{3m} \rangle_{B'B} Y_2^{km} \frac{3t}{2M_N} F_{\text{mf},2}^{u-d}, \end{aligned} \quad (40b)$$

where $F_{\text{mf},0} \equiv F_{\text{mf},0}(t)$, $F_{\text{mf},1} \equiv F_{\text{mf},1}(t)$, and $F_{\text{mf},2} \equiv F_{\text{mf},2}(t)$ represent “mean-field” form factors. Their subscripts indicate the multipole order L in Δ . We obtain the three independent multipole structures consistent with the results in Eq. (10). The explicit expressions for the soliton form factors are collected in Sec. III E.

In principle, $e^{i\Delta \cdot \hat{\mathbf{X}}}$ produces an infinite number of multipole structures and mean-field form factors. In the mean-field picture, however, the discrete and hedgehog symmetries impose constraints on the possible number of multipole structures: i) The hedgehog symmetry, enforcing the “minimally generalized” rotational symmetry, prevents the partial wave from spanning to infinity, allowing to the order of $L = 2$ in the large N_c limit. ii) Depending on a given effective QCD operator, we find that the parity allows only even or odd structures in the partial waves. iii) The time-reversal symmetry restricts the form factors to be real, which discards unphysical one in the general parameterization (2). These constraints are consistent with general discrete symmetries imposed on the covariant matrix element (cf. [50, 63, 64]). Thus we get the same number of multipole structures in Eq. (40) as in Eq. (10).

The baryon matrix element in Eq. (40) can now be reduced to the nucleon matrix element by taking the quantum number $S = T = 1/2$. From Eq. (38) the nucleon matrix elements of the spin-flavor operators are derived as

$$\begin{aligned} \langle \mathbf{1} \rangle &= \delta_{S'_3 S_3} \delta_{T'_3 T_3}, \\ \langle D^{3i} \rangle &= -\frac{1}{3} (\tau^3)_{T'_3 T_3} (\sigma^i)_{S'_3 S_3}, \end{aligned} \quad (41)$$

with Cartesian components ($i = 1, 2, 3$). From now on we will consider the proton matrix element, i.e., we set $T_3 = 1/2$. Substituting the results of Eq. (41) for the matrix element of the spin-flavor operator in Eq. (40), we arrive at the matrix element of the tensor operator between the proton states:

$$\mathcal{M}^{u+d}[i\sigma^{0k}] = Y_1^i \sqrt{-t} F_{\text{mf},1}^{u+d}, \quad (42a)$$

$$\begin{aligned} \mathcal{M}^{u-d}[i\sigma^{ij}] &= i\epsilon^{ijk} \sigma^k Y_0 2M_N F_{\text{mf},0}^{u-d} \\ &\quad - i\epsilon^{ijk} \sigma^m Y_2^{km} \frac{t}{2M_N} F_{\text{mf},2}^{u-d}, \end{aligned} \quad (42b)$$

where we suppress the notations for the spin polarizations S'_3 and S_3 in Eq. (42) to be consistent with Eq. (10). Owing to the isospin symmetry (41), we also obtain the results for the neutron. The isoscalar component of the matrix element for the neutron is the same as that for the proton. However, the isovector component of the matrix element for the neutron will have the opposite sign to that of the proton matrix element.

By comparing Eq. (10) with Eq. (42), we now observe that there is one-to-one correspondence between the usual tensor form factors and the mean-field form factors for a selected flavor component in the large N_c limit. The relations between Eqs. (10) and (42) are given by

$$\begin{aligned} H_T^{u-d} + \frac{t}{6M_N^2} E_T^{u-d} &= F_{\text{mf},0}^{u-d}, \\ H_T^{u+d} + E_T^{u+d} + 2\tilde{H}_T^{u+d} &= F_{\text{mf},1}^{u+d}, \\ \frac{1}{2} H_T^{u-d} + E_T^{u-d} &= F_{\text{mf},2}^{u-d}. \end{aligned} \quad (43)$$

On the other hand, the flavor counterparts of Eq. (42) appear as the rotational corrections in the mean-field picture, which are suppressed at least by one power of N_c . The flavor counterparts of Eq. (42) are also connected to the tensor form factors (10):

$$\begin{aligned} H_T^{u+d} + \frac{t}{6M_N^2} E_T^{u+d} &= F_{\text{mf},0}^{u+d}, \\ H_T^{u-d} + E_T^{u-d} + 2\tilde{H}_T^{u-d} &= F_{\text{mf},1}^{u-d}, \\ \frac{1}{2} H_T^{u+d} + E_T^{u+d} &= F_{\text{mf},2}^{u+d}, \end{aligned} \quad (44)$$

which are obviously zero at strictly large N_c (cf. (42)), but are non-zero only if the rotational corrections are taken into account. While we exhibit the explicit expressions of Eq. (43) in Sec. III E, the rotational corrections (44) are not considered, because we focus on the N_c behavior of the tensor form factors in the current work. The corresponding results will be discussed elsewhere.

The selection rule for determining the leading flavor components in the $1/N_c$ expansion can also be understood in a general way. The N_c scaling of the baryon matrix element in the $1/N_c$ expansion is determined by the isospin-spin quantum numbers of the t channels, so-called “ $I = J$ rule” [65–67]. This rule states that the

leading N_c structure comes from the $I = J$ components. For example, for Eq. (10a), its spin quantum number is $J = 0$, so the isoscalar component $I = 0$ appears as the leading contribution, as derived in Eq. (42a). On the other hand, Eq. (10b) has $J = 1$ for both monopole and quadrupole multipole structures. Thus, its isovector component $I = 1$ should be the leading contribution in the $1/N_c$ expansion, with which Eq. (42b) coincides. Their flavor counterparts satisfying $I \neq J$ emerge as sub-leading contributions.

D. Scaling behavior and relations

The combinations of the tensor form factors on the LHS in Eqs. (43) and (44) are not homogeneous in N_c , so they are “incomplete” relations in the sense of the $1/N_c$ expansion. To have genuine large- N_c relations in Eqs. (43) and (44), information on the separate N_c scaling of the tensor form factors is required, and we have to sort out and get rid of the subleading form factors in the $1/N_c$ expansion. The procedure of finding the relations [see Eqs. (43) and (44)] refined in the $1/N_c$ expansion is as follows: i) First we obtain the N_c scaling of the mean-field form factors. ii) Then we solve the coupled Eqs. (43) and (44) to disentangle the separate usual tensor form factors, and determine the N_c scaling of them. iii) Having determined the N_c scaling of the tensor form factors, we “reverse the logic” and express the mean-field form factors in terms of the tensor form factors. In this way, we can derive the consistent relations – optimized in the $1/N_c$ expansion – between the mean-field form factors and the usual form factors.

In the leading order of the $1/N_c$ expansion, the matrix element (36) is of the order $\mathcal{O}(N_c^2)$ for both the isoscalar and isovector components. In addition, we find that the partial wave expansion does not affect on the N_c scaling of the matrix element; see Sec III C. Thus the matrix element must produce a uniform N_c scaling of the mean-field (multipole) form factors – rooted in the same dynamical origin – in the partial wave expansions. After performing the partial wave expansion, we do obtain the uniform “natural” scalings of the mean-field form factors:

$$\left\{ F_{\text{mf},0}^{u-d}, \frac{F_{\text{mf},1}^{u+d}}{M_N}, \frac{F_{\text{mf},2}^{u-d}}{M_N^2} \right\} \sim N_c^1 \times \text{function}(t). \quad (45)$$

These form factors are independent of the nucleon mass [cf. (54)], are dimensional quantities, and have the same N_c scaling. Their dimensions are $[\text{mass}^{-L}]$, where L is the multipole order. To facilitate comparison with the tensor form factors, we present the N_c scaling in terms of the dimensionless mean-field form factors $F_{\text{mf},L}$:

$$\begin{aligned} &\{F_{\text{mf},0}^{u-d}, F_{\text{mf},1}^{u+d}, F_{\text{mf},2}^{u-d}\} \\ &\sim \{N_c^1, N_c^2, N_c^3\} \times \text{function}(t). \end{aligned} \quad (46)$$

The N_c scaling of Eq. (46) is of the order $\mathcal{O}(N_c^{L+1})$. The differences in the N_c scaling arise from the multiplication

of the nucleon mass. One should keep in mind that the N_c hierarchy between the form factors in Eq. (46) does not originate from the dynamics (rotational or translational corrections), but from kinematical adjustment. The flavor counterparts of the form factors in Eq. (46) are generally suppressed by $1/N_c$, typically one order smaller than the leading components. The N_c scaling for the flavor counterparts is inferred as:

$$\begin{aligned} & \{F_{\text{mf},0}^{u+d}, F_{\text{mf},1}^{u-d}, F_{\text{mf},2}^{u+d}\} \\ & \sim \{N_c^0, N_c^1, N_c^2\} \times \text{function}(t). \end{aligned} \quad (47)$$

While these form factors are based on a new dynamical origin, compared to Eq. (46), the differences in N_c within Eq. (47) are due to the kinematical adjustment as well.

Using the N_c scalings in Eqs. (46) and (47) and taking into account the N_c scaling of the kinematic variables (39), we rewrite Eqs. (43) and (44) with respect to the separate tensor form factors and obtain the following equations for the isovector component

$$\begin{aligned} F_{\text{mf},0}^{u-d} - \frac{t}{6M_N^2} F_{\text{mf},2}^{u-d} &= H_T^{u-d}, \\ F_{\text{mf},2}^{u-d} &= E_T^{u-d}, \\ -\frac{1}{2} F_{\text{mf},2}^{u-d} &= \tilde{H}_T^{u-d}, \end{aligned} \quad (48)$$

and for the isoscalar component

$$\begin{aligned} F_{\text{mf},0}^{u+d} - \frac{t}{6M_N^2} F_{\text{mf},2}^{u+d} &= H_T^{u+d}, \\ F_{\text{mf},2}^{u+d} &= E_T^{u+d}, \\ \frac{1}{2} F_{\text{mf},1}^{u+d} - \frac{1}{2} F_{\text{mf},2}^{u+d} &= \tilde{H}_T^{u+d}. \end{aligned} \quad (49)$$

The left-handed sides (LHS) of Eqs. (48) and (49) are now homogeneous in N_c scaling. From Eqs. (48) and (49), we can read out the separate N_c scaling of the tensor form factors as follows:

$$\begin{aligned} & \{H_T^{u-d}, E_T^{u-d}, \tilde{H}_T^{u-d}\} \\ & \sim \{N_c^1, N_c^3, N_c^3\} \times \text{function}(t), \end{aligned} \quad (50a)$$

$$\begin{aligned} & \{H_T^{u+d}, E_T^{u+d}, \tilde{H}_T^{u+d}\} \\ & \sim \{N_c^0, N_c^2, N_c^2\} \times \text{function}(t). \end{aligned} \quad (50b)$$

In addition to that, from the last two equations in Eq. (48), we obtain the non-trivial relation (cf. (48))

$$2\tilde{H}_T^{u-d} = -E_T^{u-d} + \mathcal{O}(N_c^1). \quad (51)$$

This relation can also be understood by inserting Eq. (50) into the second line of Eq. (44). On the right-handed side (RHS), the $F_{\text{mf},1}^{u-d}$ is of the order $\mathcal{O}(N_c)$. On the other hand, on the LHS, the E_T^{u-d} and \tilde{H}_T^{u-d} are of the order $\mathcal{O}(N_c^3)$, and H_T^{u-d} is of the order $\mathcal{O}(N_c^1)$. To have $\mathcal{O}(N_c^1)$ on the LHS, there must be a cancellation between E_T^{u-d}

and \tilde{H}_T^{u-d} not only in the order of $\mathcal{O}(N_c^3)$ but also in the order of $\mathcal{O}(N_c^2)$. Thus, the N_c order of the subleading correction to the relation (51) must be two powers smaller than E_T^{u-d} and \tilde{H}_T^{u-d} .

Using the logical reverse again, and considering Eqs. (48) and (49), we now express the mean-field form factors in terms of the usual tensor form factors for the leading flavor components in the $1/N_c$ expansion

$$\begin{aligned} H_T^{u-d} + \frac{t}{6M_N^2} E_T^{u-d} &= F_{\text{mf},0}^{u-d}, \\ E_T^{u+d} + 2\tilde{H}_T^{u+d} &= F_{\text{mf},1}^{u+d}, \\ E_T^{u-d} &= F_{\text{mf},2}^{u-d}, \end{aligned} \quad (52)$$

and for their flavor counterparts

$$\begin{aligned} H_T^{u+d} + \frac{t}{6M_N^2} E_T^{u+d} &= F_{\text{mf},0}^{u+d}, \\ H_T^{u-d} + E_T^{u-d} + 2\tilde{H}_T^{u-d} &= F_{\text{mf},1}^{u-d}, \\ E_T^{u+d} &= F_{\text{mf},2}^{u+d}. \end{aligned} \quad (53)$$

In the leading order of the $1/N_c$ expansion, the combination of the LHS in Eq. (52) can be regarded as alternative definitions of the tensor form factors that have homogeneous N_c scaling. For the flavor counterpart (53), we also derive the similar combination. In the perspective of the $1/N_c$ expansion, this new basis has a clear physical interpretation and will be employed in the rest of discussion in this work.

E. Tensor form factors in the mean-field picture

In the leading order of the $1/N_c$ expansion, the explicit expressions for the mean-field form factors in Eq. (40) are collected as follows:

$$\begin{aligned} F_{\text{mf},0}^{u-d} &= -\frac{N_c}{9} \sum_{n,\text{occ}} \\ & \times \langle n | \gamma^0 (\boldsymbol{\Sigma} \cdot \boldsymbol{\tau}) Y_0 j_0(|\hat{\mathbf{X}}|\sqrt{-t}) | n \rangle \Big|_{\text{reg}}, \end{aligned} \quad (54a)$$

$$\begin{aligned} F_{\text{mf},1}^{u+d} &= 2M_N N_c \sum_{n,\text{occ}} \\ & \times \langle n | \gamma^0 \gamma^5 \Sigma^i Y_1^{ij} \frac{j_1(|\hat{\mathbf{X}}|\sqrt{-t})}{\sqrt{-t}} | n \rangle \Big|_{\text{reg}}, \end{aligned} \quad (54b)$$

$$\begin{aligned} F_{\text{mf},2}^{u-d} &= -2M_N^2 N_c \sum_{n,\text{occ}} \\ & \times \langle n | \gamma^0 \Sigma^i \tau^j Y_2^{ij} \frac{j_2(|\hat{\mathbf{X}}|\sqrt{-t})}{t} | n \rangle \Big|_{\text{reg}}, \end{aligned} \quad (54c)$$

where $j_L(|\hat{\mathbf{X}}|\sqrt{-t})$ denotes the 3D spherical Bessel functions. The irreducible rank- L tensors Y_L are given as the functions of the 3D angles of the displacement operator

$\hat{\mathbf{X}}$. As already discussed, the quark states are the eigenstates of the grandspin \mathbf{G} . By coupling the first quantized operator (54) in the flavor, the spin, and the orbital angular momentum spaces, the operator can now be characterized by the grandspin quantum number. As shown in Eq. (54), these first quantized operators between the quark states $|n\rangle$ are obviously scalar functions and have no orientation in the “minimally generalized” rotation. Thus the mean-field form factors in (54) are only a function of the squared momentum transfer t (scalar).

Before discussing more about the mean-field form factors, we need to specify the relevant domain of $-t$ for them in the large- N_c limit. The squared momentum transfer scale $\Delta^2 = t = O(N_c^0)$ (cf. (39)), and its temporal component $(\Delta^0)^2$ is a subleading correction to t . Thus, the lower bound of $-t$ in the large- N_c limit is determined to be

$$|\Delta|^2 + \mathcal{O}(N_c^{-1}) = -t \geq 0. \quad (55)$$

It means that the squared momentum transfer always remains in the spacelike domain. On the other hand, $-t$ should not exceed the scale of the squared nucleon mass $M_N^2 = \mathcal{O}(N_c^2)$ in the perspective of the large- N_c limit. Thus the upper limit of $-t$ is given by

$$-t \ll M_N^2 \sim 1 \text{ GeV}^2. \quad (56)$$

Considering this N_c behavior of the momentum transfer, we determine the reliable domain for $-t$ at large N_c to be $0 \leq -t < 1 \text{ GeV}^2$. Thus, we can unambiguously take the forward limit $-t \rightarrow 0$. In this limit, the spherical Bessel function in Eq. (54) becomes

$$j_L(|\hat{\mathbf{X}}|\sqrt{-t}) \xrightarrow{t \rightarrow 0} \frac{(|\hat{\mathbf{X}}|\sqrt{-t})^L}{(2L+1)!!}, \quad (L = 0, 1, 2, \dots). \quad (57)$$

Using this asymptotic behavior of the spherical Bessel function (57), we show that the expressions of the mean-field form factors are reduced to

$$F_{\text{mf},0}^{u-d}(0) = g_T^{u-d} = -|n\rangle \Big|_{\text{reg}}, \quad (58a)$$

$$F_{\text{mf},1}^{u+d}(0) = \kappa_T^{u+d} = \frac{2M_N N_c}{3} \sum_{n,\text{occ}} \langle n | \gamma^0 \gamma^5 i \boldsymbol{\Sigma} \cdot \hat{\mathbf{X}} | n \rangle \Big|_{\text{reg}}, \quad (58b)$$

$$F_{\text{mf},2}^{u-d}(0) = -Q_T^{u-d} = \frac{2M_N^2 N_c}{15} \sum_{n,\text{occ}} \langle n | \gamma^0 \left[(\boldsymbol{\Sigma} \cdot \hat{\mathbf{X}})(\boldsymbol{\tau} \cdot \hat{\mathbf{X}}) - \frac{1}{3}(\boldsymbol{\Sigma} \cdot \boldsymbol{\tau}) \hat{\mathbf{X}}^2 \right] | n \rangle \Big|_{\text{reg}}. \quad (58c)$$

From Eq. (52), we observe that these results (58) are directly related to the tensor charge g_T^{u-d} , the anomalous tensor magnetic moment κ_T^{u+d} , and the tensor quadrupole moment Q_T^{u-d} , respectively.

To facilitate the study of the chiral properties of the tensor form factors in Eqs. (54) and (58) we need to express them in terms of the corresponding densities in coordinate space. This can be done by projecting Eqs. (54) and (58) onto the eigenstates of the displacement operator $|\mathbf{x}\rangle$. Inserting the completeness

$$\int d^3x |\mathbf{x}\rangle \langle \mathbf{x}| = 1, \quad (59)$$

into Eqs. (54) and (58), we obtain the expressions for the mean-field form factors as follows:

$$F_{\text{mf},0}^{u-d} = \int_0^\infty dr 4\pi r^2 j_0(r\sqrt{-t}) \rho_{0T}^{u-d}(r), \quad (60a)$$

$$F_{\text{mf},1}^{u+d} = 3 \int_0^\infty dr 4\pi r^2 \frac{j_1(r\sqrt{-t})}{r\sqrt{-t}} \rho_{1T}^{u+d}(r), \quad (60b)$$

$$F_{\text{mf},2}^{u-d} = 15 \int_0^\infty dr 4\pi r^2 \frac{j_2(r\sqrt{-t})}{(r\sqrt{-t})^2} \rho_{2T}^{u-d}(r), \quad (60c)$$

where the explicit expressions for the tensor densities are listed in Appendix A. In the forward limit $t \rightarrow 0$, making use of Eq. (57), we obtain the tensor charge g_T^{u-d} , the anomalous tensor magnetic moment κ_T^{u+d} , and the tensor quadrupole moment Q_T^{u-d} , respectively, defined in Eq. (58):

$$F_{\text{mf},0}^{u-d}(0) = \int_0^\infty dr 4\pi r^2 \rho_{T0}^{u-d}(r) = g_T^{u-d}, \quad (61a)$$

$$F_{\text{mf},1}^{u+d}(0) = \int_0^\infty dr 4\pi r^2 \rho_{T1}^{u+d}(r) = \kappa_T^{u+d}, \quad (61b)$$

$$F_{\text{mf},2}^{u-d}(0) = \int_0^\infty dr 4\pi r^2 \rho_{T2}^{u-d}(r) = -Q_T^{u-d}. \quad (61c)$$

F. Discrete level contribution

The tensor form factors, as discussed in Eqs. (26) and (54), comprise the contributions from both the discrete level (lev) and negative continuum levels (Dirac sea) states. The sum of these two contributions is denoted as “occ = discrete level + Dirac sea”. We begin the analysis by considering the contribution of the discrete level. The discrete level comes from the $G = 0$ and $\Pi = +$ state of the quark spectrum. The discrete-level wave function takes the following form:

$$\langle \mathbf{x} | \text{lev} \rangle = \Phi_{\text{lev}}(\mathbf{x}) = \frac{1}{\sqrt{4\pi}} \begin{pmatrix} f_0(r) \\ -i \frac{\boldsymbol{x}\boldsymbol{\sigma}}{r} f_1(r) \end{pmatrix} \chi, \quad (62)$$

The discrete-level wave function $\Phi_{\text{lev}}(\mathbf{x})$ incorporates χ , a spinor-isospinor wave function, which satisfies the hedgehog condition $(\boldsymbol{\sigma} + \boldsymbol{\tau})\chi = 0$, with the normalization $\chi^\dagger \chi = 1$. The radial components of the wave function, denoted as f_0 and f_1 , are governed by the following equa-

tion in the chiral limit ($m = 0$):

$$\begin{pmatrix} M \cos P(r) & -\frac{\partial}{\partial r} - \frac{2}{r} + M \sin P(r) \\ \frac{\partial}{\partial r} + M \sin P(r) & -M \cos P(r) \end{pmatrix} \times \begin{pmatrix} f_0(r) \\ f_1(r) \end{pmatrix} = E_{\text{lev}} \begin{pmatrix} f_0(r) \\ f_1(r) \end{pmatrix}, \quad (63)$$

where $P(r)$ is the profile function of the pion mean field, while E_{lev} represents the level-quark eigenenergy. The radial wave functions are normalized as

$$\int_0^\infty dr r^2 [f_0^2(r) + f_1^2(r)] = 1. \quad (64)$$

The subscripts of the quark wave functions $f_0(r)$ and $f_1(r)$ correspond to the orbital angular momentum quantum numbers $L = 0$ and $L = 1$, respectively. In the physical mean-field profile, the lower component f_1 accounts for approximately 20% of the normalization integral (64), indicating that relativistic contributions are small but non-negligible.

Using the discrete-level wave functions (62), we evaluate the first-quantized matrix elements in Eq. (54). The resulting discrete-level contributions to the tensor form factors are then expressed as

$$F_{\text{mf},0}^{u-d}[\text{lev}] = \frac{N_c}{3} \int_0^\infty dr j_0(r\sqrt{-t}), \quad (65a)$$

$$\times r^2 \left[f_0^2(r) + \frac{1}{3} f_1^2(r) \right],$$

$$F_{\text{mf},1}^{u+d}[\text{lev}] = -4M_N N_c \int_0^\infty dr \frac{j_1(r\sqrt{-t})}{r\sqrt{-t}}, \quad (65b)$$

$$\times r^3 [f_0(r)f_1(r)],$$

$$F_{\text{mf},2}^{u-d}[\text{lev}] = \frac{8}{3} M_N^2 N_c \int_0^\infty dr \frac{j_2(r\sqrt{-t})}{(r\sqrt{-t})^2} \quad (65c)$$

$$\times r^4 [f_1^2(r)].$$

Using (57), we can simplify the discrete-level contributions to the tensor form factors in the forward limit ($t \rightarrow 0$):

$$F_{\text{mf},0}^{u-d}(0)[\text{lev}] = \frac{N_c}{3} \int_0^\infty dr r^2 \left[f_0^2(r) + \frac{1}{3} f_1^2(r) \right], \quad (66a)$$

$$F_{\text{mf},1}^{u+d}(0)[\text{lev}] = -\frac{4}{3} M_N N_c \int_0^\infty dr r^3 [f_0(r)f_1(r)], \quad (66b)$$

$$F_{\text{mf},2}^{u-d}(0)[\text{lev}] = \frac{8}{45} M_N^2 N_c \int_0^\infty dr r^4 [f_1^2(r)]. \quad (66c)$$

We see that the monopole mean-field form factor (65a) originates from both the non-relativistic f_0 and relativistic f_1 wave functions. On the other hand, the dipole form factor (65b) arises from the mixing between the f_0 and f_1 wave functions, and the pure f_1 wave function is

responsible for the quadrupole form factor (65c). This observation emphasizes that it is crucial to consider the relativistic effects on the higher multipole structures.

The above argument can clearly be demonstrated by considering an extreme limit. In the mean-field picture, the non-relativistic (NR) limit can be reached by shrinking the average size of the pion mean field. Then the quarks interact loosely with the mean field in 3D space, so that we paint the non-relativistic picture. In this limit, the $|f_1|$ over r vanishes as expected, and the discrete-level energy is reduced to the dynamical quark mass, i.e. $E_{\text{lev}} \approx M$

$$|f_1(r)| \xrightarrow{\text{NR limit}} 0, \quad E_{\text{lev}} \xrightarrow{\text{NR limit}} M. \quad (67)$$

This means that the quarks are very weakly bound, almost like free quarks. The normalization of the quark wave function in this limit becomes

$$\int_0^\infty dr r^2 f_0^2(r) = 1. \quad (68)$$

Under these conditions (67) and (68), the mean-field form factors (65) are remarkably simplified as

$$F_{\text{mf},0}^{u-d}(0)[\text{lev}] = \frac{N_c}{3} \int_0^\infty dr r^2 f_0^2(r) = \frac{N_c}{3}, \quad (69a)$$

$$F_{\text{mf},1}^{u+d}(0)[\text{lev}] = 0, \quad (69b)$$

$$F_{\text{mf},2}^{u-d}(0)[\text{lev}] = 0. \quad (69c)$$

These results demonstrate that in the NR limit, only the tensor charge (69a) survives with a constant value¹ $g_T^{u-d}[\text{lev}] = N_c/3$, while both the dipole $\kappa_T^{u+d}[\text{lev}] = 0$ and quadrupole $Q_T^{u-d}[\text{lev}] = 0$ moments vanish. The NR limit highlights the significance of relativistic effects to describe the tensor structure of nucleon, particularly for higher-order multipoles.

G. Gradient expansion

We now examine how the Dirac sea affects the mean-field form factors. The Dirac sea contribution, unlike the discrete level contribution, cannot be expressed analytically. It involves the summation of countless overlapping quark wave functions, each characterized by quantum numbers (such as energy, grandspin, and parity).

¹ In the non-relativistic quark model, the tensor charge is the same as the axial charge g_A^{u-d} , and is known as $(N_c + 2)/3$. In the leading order of the $1/N_c$ expansion only part of the results $N_c/3$ can be explained. The rest of them $\sim 2/3$ arises from the sub-leading order contributions (see Refs. [51, 52]). In this work, we restrict ourselves into the strict large N_c .

Before we compute the Dirac-sea contributions, we examine the behavior of the tensor form factors by using the gradient expansion, which is valid in the limit of the large mean-field size. This is called the Skyrme limit, since the expressions in the nonvanishing leading-order are identical with the results from the simplest version of the Skyrme model that contains only the Weinberg and Gasser-Leutwyler (Skryme) Lagrangians [68]. Thus, the current theoretical framework has a merit of interpolating between the NR and Skyrme limits [47, 48].

The gradient expansion can be performed by the following procedure. Since a three-point correlation function is given in terms of the quark propagator given as

$$G(x, y|U) = -\langle x | \frac{1}{i\cancel{\partial}_{\hat{x}} - MU\gamma_5(\hat{x})} | y \rangle, \quad (70)$$

we can expand it in powers of the gradient of the chiral field ($\partial U \ll M$), whose expansion is also known as the chiral expansion, since it is compatible with the expansion in powers of the pion momentum. By considering the nonvanishing leading term in the expansion, we can evaluate the nucleon matrix element in terms of the chiral field. The gradient expansion yields analytical expressions for the nucleon matrix elements, approximating the total matrix element including both the discrete level and the Dirac sea contributions. They reveal the chiral properties (large distance behavior) of the corresponding nucleon matrix element in the large N_c limit.

The gradient expansion provides us with two main advantages. First, as discussed above, it provides theoretical insight into chiral properties of the 3D densities in the long range regime (60) (so-called the Yukawa tail). Understanding the large r behavior allows for extrapolation of 3D distributions, thereby mitigating unwanted finite box effects in numerical calculation. Second, the low-energy constants for effective chiral Lagrangian are explicitly derived by performing the quark-loop integral, revealing the UV divergence pattern of a relevant physical quantity. Thus, we can determine whether we have to introduce a regularization scheme to tame the corresponding UV divergence [69]².

Keeping these features in mind, we apply the gradient expansion to the nucleon matrix element of the tensor operator (35), and obtain the leading-order contributions to the mean-field form factors in the chiral limit ($m_\pi = 0$)

² For example, while the pion decay constant is logarithmically divergent, the Gasser-Leutwyler low-energy constants for the effective chiral Lagrangian to the order $\mathcal{O}(p^4)$ are UV stable [44, 70]. A similar consideration can be done also in the case of various nucleonic observables.

and in the $1/N_c$ and chiral expansions³:

$$\begin{aligned} F_{\text{mf},0}^{u-d}[\text{grad}] &= -\frac{MN_c}{288\pi^2} \int d^3r j_0(r\sqrt{-t}) i\epsilon^{ijk} \\ &\quad \times \text{tr}[L_i L_j (\tau^k U + U^\dagger \tau^k) - (i \leftrightarrow j)], \\ F_{\text{mf},1}^{u+d}[\text{grad}] &= \frac{M_N M N_c}{8\pi^2} \int d^3r \frac{j_1(r\sqrt{-t})}{r\sqrt{-t}} \epsilon^{ijk} r^k \\ &\quad \times \text{tr}[(U - U^\dagger) L_i L_j], \\ F_{\text{mf},2}^{u-d}[\text{grad}] &= \frac{M_N^2 M N_c}{16\pi^2} \int d^3r \frac{j_2(r\sqrt{-t})}{(r^2\sqrt{-t})^2} (r^l r^k - \frac{1}{3}\delta^{lk} r^2) \\ &\quad \times i\epsilon^{ijl} \text{tr}[L_i L_j (\tau^k U + U^\dagger \tau^k) - (i \leftrightarrow j)], \end{aligned} \quad (71)$$

where the trace, $\text{tr}[\dots]$, runs over flavor space and the left chiral current L is defined by

$$L_\mu := U^\dagger \partial_\mu U. \quad (72)$$

Note that these results arise from the non-divergent quark-loop integrals. Thus, all tensor form factors are UV finite, eliminating the need for any regularization scheme. The physical reason for this lies in the fact that matrix element of the tensor operator solely originates from the anomalous part of the fermionic determinant⁴; see Appendix A for details.

We employ the arctangent profile function with the pion Yukawa tail introduced:

$$P(r) = 2 \arctan \left[\frac{R^2}{r^2} (1 + m_\pi r) e^{-m_\pi r} \right], \quad (73)$$

where R is the average size of the pion mean field, which can be considered as a variable. The physical value of R is approximately given as $MR \approx 1$ [44]. Note that the soliton size R can be reexpressed in terms of the axial charge $g_A = 1.26$ and the pion decay constant $f_\pi = 93$ MeV in the chiral limit (see Ref. [71])

$$R = \sqrt{\frac{3g_A}{16\pi f_\pi^2}} [m_\pi = 0]. \quad (74)$$

This expression allows one to connect the present results with those from chiral perturbation theory [71, 72]. Expanding the profile function (73) for large r reproduces

³ We started with the effective chiral action, as described in Eq. (19), assuming a zero current quark mass ($\hat{m} = 0$). We then performed a gradient expansion, which finally leads to the expression given in Eq. (71). It is important to note that the inclusion of effects from explicit chiral symmetry breaking in the effective chiral action may introduce additional contributions to the current study (71). However, for the sake of simplicity in this study, we have not included these effects.

⁴ Reference [53] employed the proper-time regularization scheme to estimate the anomalous tensor magnetic moment κ_T^{u+d} . However, they introduced the regularization functions in an inconsistent way.

the correct pion Yukawa tail:

$$P(r) \underset{r \rightarrow \infty}{=} \frac{2R^2}{r^2} + \dots, \quad [m_\pi = 0],$$

$$P(r) \underset{r \rightarrow \infty}{=} \frac{2R^2}{r^2} (1 + m_\pi r) e^{-m_\pi r} + \dots, \quad [m_\pi \neq 0], \quad (75)$$

where the ellipses indicate subleading contributions.

Since the chiral field (75) has a correct large r behavior, it is legitimate to examine the large r behavior of the 3D distributions (60) with this chiral field (73). By inserting Eq. (75) into Eq. (71), we obtain the asymptotic forms of the 3D distributions (60) for a finite pion mass:

$$\rho_{0T}(r) \underset{r \rightarrow \infty}{=} \frac{2MN_c R^4}{3\pi^2 r^6} e^{-2m_\pi r} \times (3 + 4m_\pi r + m_\pi^2 r^2) + \dots, \quad (76a)$$

$$\rho_{1T}(r) \underset{r \rightarrow \infty}{=} \frac{8MM_N N_c R^6}{3\pi^2 r^7} e^{-3m_\pi r} \times (1 + 3m_\pi r + 3m_\pi^2 r^2 + m_\pi^3 r^3) + \dots, \quad (76b)$$

$$\rho_{2T}(r) \underset{r \rightarrow \infty}{=} \frac{8MM_N^2 N_c R^4}{15\pi^2 r^4} e^{-2m_\pi r} \times \left(1 + \frac{5}{3}m_\pi r + \frac{2}{3}m_\pi^2 r^2\right) + \dots \quad (76c)$$

These expressions show the influence of the finite quark mass on the long-range behavior of the distributions. In the chiral limit ($m_\pi \rightarrow 0$), these distributions simplify to

$$\rho_{0T}^{u-d}(r) \underset{r \rightarrow \infty}{=} \frac{2MN_c R^4}{\pi^2 r^6}, \quad (77a)$$

$$\rho_{1T}^{u+d}(r) \underset{r \rightarrow \infty}{=} \frac{8MM_N N_c R^6}{\pi^2 r^7}, \quad (77b)$$

$$\rho_{2T}^{u-d}(r) \underset{r \rightarrow \infty}{=} \frac{8MM_N^2 N_c R^4}{15\pi^2 r^4}. \quad (77c)$$

In particular, the dipole distribution ρ_{1T} falls off, being proportional to $1/r^7$ in large r , while the monopole ρ_{0T} and quadrupole ρ_{2T} distributions decrease as $1/r^6$ and $1/r^4$, respectively. Note that the quadrupole tensor distribution diminishes less than the monopole and dipole ones, so the strong chiral enhancement is expected for the quadrupole tensor moment Q_T^{u-d} in the chiral limit compared to the tensor charge and anomalous tensor magnetic moment.

By inserting the arctangent profile function (73) into Eq. (71), the mean-field form factors can be expressed in terms of R in the chiral limit:

$$F_{\text{mf},0}^{u-d}(0)[\text{grad}] = \frac{5N_c M R}{12\sqrt{2}}, \quad (78a)$$

$$F_{\text{mf},1}^{u+d}(0)[\text{grad}] = \frac{4M_N M N_c R^2}{3\pi}, \quad (78b)$$

$$F_{\text{mf},2}^{u-d}(0)[\text{grad}] = \frac{11M_N^2 M N_c R^3}{15\sqrt{2}}. \quad (78c)$$

These expressions reveal that the multipole mean-field form factors $F_{\text{mf},L}$ with the multipole order L are proportional to R^L . This relationship indicates that higher multipole form factors exhibit a stronger dependence on R . Consequently, it is crucial to determine R accurately by a self-consistent calculation, in particular, for the higher multipole form factors. Utilizing the physical profile function with $MR \approx 1$ in Eq. (78), we derive the following numerical values for the tensor moments:

$$g_T^{u-d}[\text{grad}] = 0.88,$$

$$\kappa_T^{u+d}[\text{grad}] = 4.25,$$

$$Q_T^{u-d}[\text{grad}] = -17.38. \quad (79)$$

where we employ the nucleon mass of $M_N = 1170$ MeV [44], as determined in the chiral limit.

IV. NUMERICAL RESULTS

So far, we have examined the physical features of the tensor form factors. We now evaluate the tensor form-factors based on the self-consistent calculation. Before discussing the numerical results, we briefly show how we determine the parameters. First, the dynamical quark mass is taken to be $M = 350$ MeV, which is approximately determined from the QCD instanton vacuum. Here we employ the proper-time regularization scheme with a cutoff mass Λ . By reproducing the experimental value of the pion decay constant $f_\pi = 93$ MeV and the pion mass $m_\pi = 140$ MeV, we simultaneously fix the current quark mass m and Λ (see Refs. [49, 73] for details):

$$m = 16 \text{ MeV}, \quad \Lambda = 643 \text{ MeV}, \quad (80)$$

where the magnitude of the UV cutoff mass Λ is indeed comparable to the inverse of the average instanton size $\bar{\rho}^{-1} \approx 600$ MeV. As mentioned in Eq. (26), the classical nucleon mass is a logarithmically divergent quantity and should be regularized. With (80) used, we obtain the classical nucleon mass to be

$$M_N = 1254 \text{ MeV}. \quad (81)$$

Evaluating the nucleonic observables, we find that the finite box size brings about numerical uncertainty near the boundary of the box (60). To avoid this uncertainty, we replace the tail part of the densities with those derived from the gradient expansion (71) at large r (typically around 1 – 2 fm). This process effectively restores the chiral properties in the numerical results. This method allows for a more accurate numerical study of the chiral properties of tensor form factors in the large N_c limit of QCD. It has proven particularly valuable in examining the stability condition and verifying the negativity of the D -term form factor, as demonstrated in previous studies [71, 74, 75].

We find that the discrete-level contributions to the tensor charge and anomalous tensor magnetic moment dominate over the Dirac-continuum contributions, as shown in

	Level	Dirac Sea	Total	Gradient ($m_\pi = 0$)
g_T^{u-d}	0.88	0.11	0.99	0.88
κ_T^{u+d}	6.92	0.69	7.61	4.25
$-Q_T^{u-d}$	3.08	3.94	7.02	17.38

TABLE I. Numerical results for the isovector tensor charge g_T^{u-d} , isoscalar anomalous tensor magnetic moment κ_T^{u+d} , and isovector tensor quadrupole moment with the physical pion mass $m_\pi = 140$ MeV employed. The results are also compared to those from the gradient expansion in the chiral limit.

Table I. While the discret level yields $g_T^{u-d}[\text{lev}] = 0.88$, the Dirac continuum contributes to it only by around 10% [51, 52, 76]. Similarly, the isoscalar anomalous tensor magnetic moment κ_T^{u+d} is primarily governed by the discrete level ($\kappa_T^{u+d}[\text{lev}] = 6.92$). Again, the Dirac continuum gives only $\approx 10\%$ of κ_T^{u+d} . On the other hand, the tensor quadrupole moment exhibits significant Dirac-sea contribution ($\gtrsim 50\%$), which is in line with the case of the electric quadrupole moment [77] and D -term form factor [71, 75]. Note that if one considers only the valence-quark (discrete-level) contributions, results for D -term is underestimated by the experimental data [78]. Thus, the Dirac continuum (sea quarks) must be considered to confront with the data. These findings imply that relativistic quantum field-theoretical approaches are essential for accurate description of the nucleon structure, particularly for explaining the quadrupole moments quantitatively.

The numerical values of the tensor charge and anomalous tensor magnetic moment have been previously estimated in Refs. [51, 52] and Ref. [53], respectively, within the same mean-field picture but with a different accuracy. The current results reproduce the tensor charges obtained from Refs. [51] in the strict large N_c limit. Concerning the anomalous tensor magnetic moment [53], we find that while the discrete-level contributions are in agreement with those from Ref. [53], we have the different results from the Dirac continuum:

$$\begin{aligned} \kappa_T^{u+d}[\text{sea}] &= 0.05 \quad (\text{Regularized [53]}), \\ \kappa_T^{u+d}[\text{sea}] &= 0.69 \quad (\text{Non-regularized}). \end{aligned} \quad (82)$$

This discrepancy stems from the inconsistent regularization scheme employed by Ref. [53].

Reference [40] estimated the isovector tensor charge of the nucleon to be $g_T^{u-d} = 0.97(3)(2)_{\text{sys}}$, using 2 + 1-flavor Wilson-clover fermions in lattice QCD. On the other hand, Alexandrou et al. [41] used the twisted mass fermions ($N_f = 2 + 1 + 1, m_\pi = 260$ MeV) to obtain $g_T^{u-d} = 1.11(2)$. The current results are in good agreement with these lattice data. However, quark model predictions overestimate them [21, 27]. Considering the fact that the tensor quadrupole moment is identified as one of the first moment of the chiral-odd GPDs. A recent investigation in lattice QCD [79] supports the large N_c relations (51), which were for the first time derived from

Ref. [50].

The multipole tensor moments were extracted also from GPDs computed within the MIT bag model [27]: $g_T^{u-d} \approx 1.38$, $\kappa_T^{u+d} \approx 6.06$, $Q_T^{u-d} \approx -5$, which are comparable to those presented above. Notably, results for the tensor form factors in the forward limit $\tilde{H}_T(0) \approx -2.6$ and $E_T(0) \approx 6.1$ follow the large N_c relation [27]:

$$2\tilde{H}_T^{u-d} \approx -E_T^{u-d}. \quad (\text{bag model [27]}). \quad (83)$$

The light-front quark model with the hypercentral potential [21] yields $g_T^{u-d} \approx 1.21$ and $\kappa_T^{u+d} \approx 3.15$. While tensor charges are in close agreement with the current results, the anomalous tensor magnetic moment is underestimated by about 50%, compared with the present prediction. The basis light-front quantization model [80] produces a larger value of the tensor charge ($g_T^{u-d} \approx 1.52$) but the value of the anomalous tensor magnetic moment ($\kappa_T^{u+d} \approx 5.64$) is closer to our result.

The tensor moments are scale-dependent. Thus, it is of great significance to consider the scale evolution for the tensor moments. At the one-loop level, the expression for the scale evolution was derived in Refs. [81, 82]:

$$g_T^q(\mu^2) = \left(\frac{\alpha_s(\mu^2)}{\alpha_s(\mu_0^2)} \right)^{\frac{4}{33-2N_f}} g_T^q(\mu_0^2), \quad (84)$$

which shows a weak dependence on the scale. This equation can also be applied to the anomalous tensor magnetic moment and quadrupole moments, since they come from the same tensor operator. As the scale increases towards infinity $\mu \rightarrow \infty$, the tensor charge slowly approaches zero. While it is relatively stable across different scales, this scale dependence does introduce some uncertainty in our calculations. Since the present effective chiral theory is based on the QCD instanton vacuum, the intrinsic scale is naturally determined by the average instanton size, is set at $\mu_0 \approx \bar{\rho}^{-1} = 600$ MeV [51]. To maintain consistency with the large N_c approximation and avoid additional assumptions, we present the results at the intrinsic scale given above. For more advanced treatments, two-loop and three-loop evolution expressions are available in literatures [83, 84].

V. DISCUSSION

A. Non-relativistic quark model vs. the Skyrme model

Previously, we showed that the derivative expansion demonstrates approximately the Skyrme picture of the present mean-field theory at its large average size R . If we take the opposite limit, i.e., $R \rightarrow 0$, we are able to interpolate between the non-relativistic quark model (NRQM) limit and the Skyrme limit. Both the limits can be regarded as two extreme limits of the current pion mean-field theory.

When $R \ll M^{-1}$, massive quarks become weakly bound by the mean field, with discrete-level energy approximate to the dynamical quark mass, $E_{\text{lev}} \approx M$, and vacuum polarization effects become negligible ($E_{\text{sea}} \approx 0$). It means that the mean field approaches a non-relativistic quark limit, i.e., $M_N \approx N_c M$. In this regime, it exhibits properties consistent with the NRQM.

Conversely, when $R \gg M^{-1}$, the discrete-level quarks get strongly bound, so that the discrete-level energy turns negative, $E_{\text{lev}} < 0$. Then, they finally dive into the Dirac sea, and the baryon number of the nucleon comes solely from the Wess-Zumino-Witten term, which is derived by the gradient expansion of the imaginary part of the effective chiral action (19). Thus, the baryon number is identified as the topological winding number, and the topological soliton emerges from the strongly polarized Dirac-sea vacuum. This picture exactly corresponds to what Witten suggested [45]. In this limit of $MR \gg 1$, the Dirac-continuum energy approaches to the nucleon mass ($E_{\text{sea}} \approx M_N$).

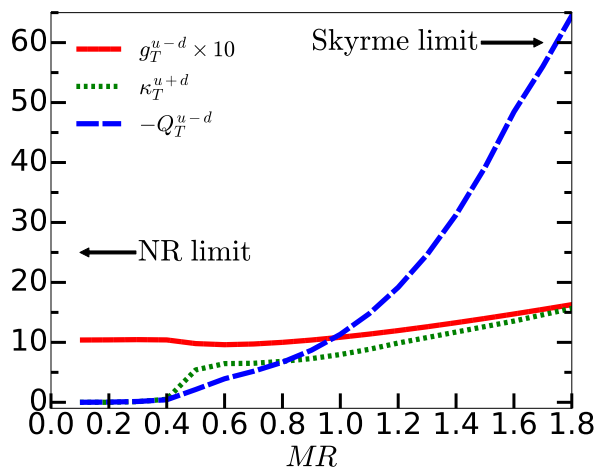


FIG. 1. Tensor multipole moments computed with the arctangent profile function (73) as a function of the dimensionless parameter MR . *Solid curve*: tensor charge. *Dotted one*: anomalous tensor magnetic moment. *Dashed one*: tensor quadrupole moment.

We now compute the tensor multipole moments, employing the arctangent profile function instead of the self-consistent one with the dimensionless parameter MR varied. The results are depicted in Fig. 1, which shows three distinct regimes. For $MR < 0.5$ the quarks are nearly unbound, leading to a plateau. The self-consistent solution for the pion mean field appears at about $MR \approx 1$. When MR reaches about 1.5, the discrete level quark merges with the Dirac sea. Examining these results, we have the following observations:

- (i) As R decreases below the physical value ($MR < 1$), the tensor charge $g_T^{u-d}[\text{lev}]$, proportional to $f_0^2 + (1/3)f_1^2$, remains almost stable. This stability results from the dominance of the non-relativistic

component f_0 in the wave function, with the relativistic component f_1 contributing only a small correction of at most 20% to the tensor charge. In addition, the contribution of the Dirac continuum is negligible in this region. Consequently, the value of g_T^{u-d} for $MR \approx 1$ is very close to that from the NRQM ($MR < 0.5$), which suggests the validity of the NRQM prediction for the tensor charge g_T^{u-d} .

In contrast, κ_T^{u+d} shows a dramatic change around $MR \approx 0.5$. This behavior is attributed to its dependence on the mixed product of the upper and lower components ($f_0 f_1$) in the discrete level contribution, and to the fact that the Dirac continuum contributes only marginally to κ_T^{u+d} . As the pion mean field approaches an unbound state ($|f_1| = 0$), κ_T^{u+d} decreases sharply due to the decreasing $|f_1|$ component.

Q_T^{u-d} , which is proportional to f_1^2 in the discrete-level contribution, exhibits a purely relativistic effect. In addition, there is a huge Dirac-continuum contribution, which increases rapidly as MR increases. It reflects the sensitivity of Q_T^{u-d} to relativistic and Dirac-continuum effects.

These numerical observations are consistent with the analytical properties described in Eq. (69), which predicts that both Q_T^{u-d} and κ_T^{u+d} approach zero in the non-relativistic limit.

- (ii) As R increases from the physical one, i.e. $MR > 1$, the values of the tensor multipole moments increase. The reason can be found in the fact that the relativistic effects in the discrete level get stronger and the contribution from the Dirac continuum becomes sizable.
- (iii) In the regime where $MR \gg 1$, the behavior of the tensor multipole moments is consistent with the predictions from the gradient expansion, as explained in Eq. (78). The dependence of these moments on MR can be characterized as follows:

$$\begin{aligned} g_T^{u-d} &\sim (MR)^1, \\ \kappa_T^{u+d} &\sim (M_N R)^1 (MR)^1, \\ Q_T^{u-d} &\sim (M_N R)^2 (MR)^1. \end{aligned} \quad (85)$$

Here, M_N is held constant. These dependence shows distinct behaviors for different tensor moments as MR increases. The tensor charge g_T^{u-d} exhibits weak dependence on MR , whereas higher tensor multipole moments are strongly enhanced on account of additional R -dependence: $k_T^{u+d} \propto R^2$ and $Q_T^{u-d} \propto R^3$. Consequently, these higher moments are significantly amplified in the large MR region.

This analysis reveals the transition in nucleon structure from non-relativistic to relativistic regimes as the

mean-field size R varies. It indicates how the tensor moments evolve differently with R , providing insight into which of the non-relativistic, relativistic, and Dirac-continuum effects is the main source of the values of the tensor moments.

B. Pion mass dependence

To study the chiral properties of the tensor form factors, we compute the tensor moments with the pion mass varied. This will shed light on the chiral extrapolation used in lattice QCD. Moreover, it is necessary to compare the present results with those of lattice QCD in which an unphysical pion mass is often used.

To consider different values of the pion mass, we repeat the procedure of fixing the cutoff and current quark masses, and derive the corresponding pion mean fields. We strictly follow Ref. [73] to obtain the pion mass dependence of the tensor form factors (see Section V). The re-

m_π	$g_T^{u-d}[\text{lev}]$	$g_T^{u-d}[\text{sea}]$	$g_T^{u-d}[\text{tot}]$
0	0.885	0.117	1.002
10	0.885	0.117	1.002
50	0.884	0.114	0.998
140	0.882	0.106	0.988
300	0.882	0.091	0.973
600	0.897	0.065	0.962
m_π	$\kappa_T^{u+d}[\text{lev}]$	$\kappa_T^{u+d}[\text{sea}]$	$\kappa_T^{u+d}[\text{tot}]$
0	6.87	0.94	7.81
10	6.87	0.94	7.81
50	6.88	0.88	7.76
140	6.92	0.69	7.61
300	6.86	0.51	7.37
600	6.66	0.43	7.09
m_π	$-Q_T^{u-d}[\text{lev}]$	$-Q_T^{u-d}[\text{sea}]$	$-Q_T^{u-d}[\text{tot}]$
0	3.01	9.58	12.59
10	3.01	8.40	11.42
50	3.03	6.21	9.24
140	3.08	3.94	7.02
300	3.01	2.73	5.74
600	2.80	2.50	5.30

TABLE II. The tensor multipole moments as functions of the pion masses.

sults for the dependence of the tensor multipole moments on m_π are summarized in Table II. We observe that the tensor moments g_T^{u-d} and κ_T^{u+d} show only weak dependence on the pion mass. As m_π increases, the discrete-level contributions to these tensor moments remain almost unchanged. However, the Dirac sea contributions diminishes as m_π increases. This can be understood that the heavier pion suppresses the mean field at large r . Thus, the discrete-level contributions remain dominant for g_T^{u-d} and κ_T^{u+d} , resulting in relatively stable total

tensor moments with the pion mass changed. In contrast, Q_T^{u-d} arises purely from the relativistic effects, as discussed in our analysis of MR dependence. For this quadrupole moment, the Dirac-continuum contribution dominates over the discrete level contribution. Consequently, Q_T^{u-d} weakens as m_π increases. This implies that Q_T^{u-d} becomes significantly enhanced in the chiral limit. This observation is indeed consistent with the result $Q_T^{u-d} = -17.38$ from the gradient expansion in the chiral limit.

This feature emphasizes the unique nature of Q_T^{u-d} among the tensor moments and underlines the importance of chiral dynamics. We anticipate results from lattice QCD in the near future, which will reveal the nature of the tensor quadrupole moments.

C. t dependence

The tensor multipole moments are just the values of the corresponding tensor form factors at $t = 0$. We now consider the t -dependence of the form factors. Due to the large N_c hierarchy between the kinematical variables, we restrict ourselves into the kinematic region where $0 \leq -t < 1 \text{ GeV}^2$ [cf. Sec.III E].

Figure 2 draw the t dependence of the tensor form factors. For the H_T^{u-d} and $E_T^{u+d} + 2\tilde{H}_T^{u+d}$, the contribution of the Dirac continuum monotonically decreases as t increases. It means that dynamical information is mostly determined by the discrete-level quarks. However, when it comes to E_T^{u-d} , the Dirac continuum takes charge over it. The dashed curve in the bottom panel of Fig. 2 shows the contribution of the Dirac continuum to E_T^{u-d} , which is larger than the discrete-level one over the whole t region. It reflect the fact that the tensor quadrupole form factor mainly is governed by the Dirac continuum. Note that \tilde{H}_T^{u-d} is equal to $-\frac{1}{2}E_T^{u-d}$ in the large N_c limit.

VI. SUMMARY AND EXTENSIONS

In this study, we aimed at investigating the nucleon tensor form factors in a pion mean-field approach, which is based on the large N_c limit and the effective chiral dynamics resulting from spontaneous chiral symmetry breaking. At large N_c the nucleon emerges as a mean-field solution of the classical equation of motion. After the zero-mode quantization, we were able to evaluate the nucleon matrix elements of the local tensor operator. Our key findings are as follows:

- (i) We perform the multipole expansion of the nucleon matrix element of the tensor operator in the mean-field picture and derive, in the $1/N_c$ expansion, its spin-flavor structure and the corresponding the mean-field form factors. These form factors are matched with the usual tensor form factors by considering the comprehensive large- N_c analysis. As

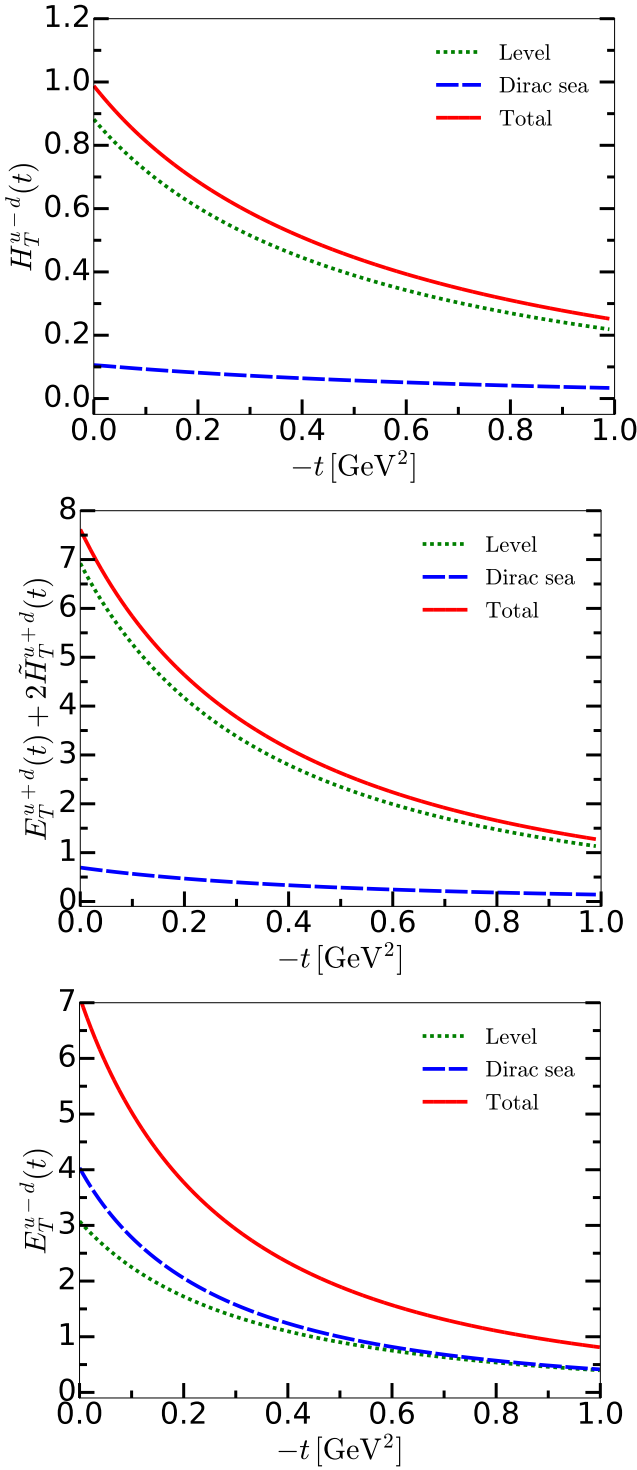


FIG. 2. The t -dependence of the tensor form factors (H_T^{u-d} , $E_T^{u+d} + 2\tilde{H}_T^{u+d}$, E_T^{u-d}). *Solid curve*: Total (discrete level + Dirac sea) contributions. *Dashed one*: Dirac sea contributions. *Dotted one*: Discrete level contributions.

a result, we determine the N_c scaling (50) of the tensor form factors and obtain the non-trivial large N_c relation (51).

- (ii) We evaluated the tensor charge ($g_T^{u-d} = 0.99$), the anomalous tensor magnetic moment ($\kappa_T^{u+d} = 7.61$), and the tensor quadrupole moment ($Q_T^{u-d} = -7.02$) with the physical pion mass; see Table I. Our results show that the tensor charge and the anomalous tensor magnetic moment are dominated by valence (discrete-level) quark contributions. On the other hand, the tensor quadrupole moment comes from the purely relativistic effects and shows significant sea (Dirac-continuum) quark effects, highlighting the importance of chiral dynamics in its description.
- (iii) Having changed the average size of the pion mean field R , we investigated how the current mean-field approach interpolates between the non-relativistic quark model and the Skyrme model. We focus on two extreme cases: for small R ($R \ll M^{-1}$), the present approach yields the picture of the non-relativistic quark model, whereas for large R , it is reduced to the Skyrme picture. Our results show that the tensor charge g_T^{u-d} from non-relativistic quark model remains rather accurate due to small relativistic and Dirac sea effects. In the non-relativistic limit, the anomalous tensor magnetic moment κ_T^{u+d} tends to zero due to the fact that the discrete-level contribution comes only from the relativistic effects and the Dirac-sea effect is negligible. However, the tensor quadrupole moment Q_T^{u-d} not only vanishes in the non-relativistic limit, but also exhibits substantial Dirac-sea contributions. This indicates that a field-theoretic approach is crucial for an accurate study of the quadrupole moment.
- (iv) We investigate the chiral properties of nucleon tensor form factors with the pion mass varied, enabling comparisons with lattice QCD results at unphysical pion masses. The results show that tensor moments g_T^{u-d} and κ_T^{u+d} exhibit weak pion mass dependence, with dominant discrete-level contributions remaining stable. In contrast, the tensor quadrupole moment Q_T^{u-d} , which arises from the relativistic effects, is dominated by Dirac-sea contributions, so that it is significantly enhanced near the chiral limit. This distinctive behavior of Q_T^{u-d} underscores the importance of chiral dynamics in tensor moments.

The spin-flavor symmetry we have explored also allows us to relate the present results to $N \rightarrow \Delta$ transition and Δ baryon tensor form factors [62, 85]. Extending the present method to flavor SU(3), we can compute the tensor form factors for the baryon octet and decuplet.

ACKNOWLEDGMENTS

JYK wants to express the gratitude to H.D. Son and C. Weiss for valuable discussion. HChK expresses his gratitude to Cédric Lorcé for valuable discussion and hospitality during his visit to Le Centre de Physique Théorique (CPHT) at École polytechnique, where part of the present work was done. He is also grateful to the members of the CPHT for their warm welcome. The work was supported by the Basic Science Research Program through the National Research Foundation of Korea funded by the Korean government (Ministry of Education, Science and Technology, MEST), Grant-No. 2021R1A2C2093368 and 2018R1A5A1025563 (NYGh and HChK). HYW acknowledges France Excellence scholarship through Campus France funded by the French government (Ministère de l'Europe et des Affaires Étrangères), Grant No. 141295X. This material is based upon work supported by the U.S. Department of Energy, Office of Science, Office of Nuclear Physics under contract DE-AC05-06OR23177.

Appendix A: 3D distributions of the tensor structure

We list the explicit expressions of the 3D distributions:

$$\rho_{0T}(r) = \frac{N_c}{9\sqrt{3}} \left(\langle v|r \rangle \{O_{0T}\}_0 \langle r|v \rangle + \sum_n \text{sign}(E_n) \frac{G(n)}{2} \langle n|r \rangle \{O_{0T}\}_0 \langle r|n \rangle \right), \quad (\text{A1a})$$

$$\rho_{1T}(r) = \frac{2i}{\sqrt{3}} M_N N_c \left(\langle v|r \rangle \{O_{1T}\}_0 \langle r|v \rangle - \sum_n \text{sign}(E_n) \frac{G(n)}{2} \langle n|r \rangle \{O_{1T}\}_0 \langle r|n \rangle \right), \quad (\text{A1b})$$

$$\rho_{2T}(r) = \frac{2M_N^2 N_c}{15\sqrt{6}} \left(\langle v|r \rangle \{O_{2T}\}_0 \langle r|v \rangle - \sum_n \text{sign}(E_n) \frac{G(n)}{2} \langle n|r \rangle \{O_{2T}\}_0 \langle r|n \rangle \right), \quad (\text{A1c})$$

where the discrete-level wave function (62) is denoted by $|v\rangle \equiv |\text{lev}\rangle$ and $G(n) = \sqrt{2G_n + 1}$. The irreducible rank-0 first-quantized operators are defined by

$$\begin{aligned} \{O_{0T}\}_0 &= \{\sigma \otimes \tau\}_0 \gamma^0, \\ \{O_{1T}\}_0 &= \{\sqrt{4\pi r} Y_1 \otimes \sigma\}_0 \gamma^5 \gamma^0, \\ \{O_{2T}\}_0 &= \left\{ \left\{ \sqrt{4\pi r^2} Y_2 \otimes \sigma \right\}_1 \otimes \tau \right\}_0 \gamma^0. \end{aligned} \quad (\text{A2})$$

The regularization function coming from the imaginary part of the fermionic determinant is merely a “sign” function in Eq. (A1), which effectively does nothing to the regularization. Thus, this result is consistent with the prediction (71) of the gradient expansion.

Appendix B: Intermediate cutoff and extrapolation

The explicit sum over the occupied quark states (26) is defined by

$$\sum_{n,\text{occ}} \langle n|\dots|n\rangle \equiv \sum_{E_n, G, G_3, \Pi} \langle n|\dots|n\rangle, \quad (\text{B1})$$

where the quark state $|n = \{E_n, G, G_3, \Pi\}\rangle$ is characterized by the energy, the grand spin, and the parity quantum number. The numerical calculations involve summation over the quark energies $-\infty < E_n < \infty$. In this section we will show how to do the sum over the quark energies numerically. There are two different way of dealing with this energy sum.

Unrefined method (conventional method): By introducing a finite range defined by $-k_{\text{max}} < E_n < k_{\text{max}}$, the energy sum can be implemented numerically. The tensor form factors are stabilized when k_{max} reaches approximately 4 GeV. As explored in the gradient expansion, the quark-loop integral is UV finite. All results in this work are obtained in this way.

Refined method: On the other hand, by introducing a varied intermediate cutoff Λ_{int} instead of k_{max} , one evaluates the tensor factors for a given range $-\Lambda_{\text{int}} < E_n < \Lambda_{\text{int}}$ where $\Lambda_{\text{int}} \ll k_{\text{max}}$. Then extrapolate these results for the tensor form factors to those with $\Lambda_{\text{int}} \rightarrow \infty$. This approach may allow a more rigorous treatment of the UV behavior of the quark momenta. However, as noted in Ref. [76], the intermediate cutoff leads to an inequivalence between occupied and non-occupied sums:

$$\sum_{n,\text{occ}} \langle n|O|n\rangle \neq - \sum_{n,\text{non}} \langle n|O|n\rangle \quad (\text{B2})$$

This equivalence is necessary for maintaining the correct positivity condition for parton distribution functions. The inequivalence arises due to the finite box size and is suppressed when $m_\pi D_{\text{box}} \ll 1$. To mitigate these artifacts, the following procedure is employed:

- (i) Evaluate tensor distributions by varying intermediate cutoffs $\Lambda_{\text{int}} \ll k_{\text{max}}$ where equivalence is preserved (i.e., fixed large pion mass $m_\pi \sim 100 - 200$ MeV)
- (ii) Extrapolate to $\Lambda_{\text{int}} \rightarrow \infty$
- (iii) Repeat for different pion masses and extrapolate to a small pion mass.

In this way we obtain the extrapolated tensor multipole moments at $\Lambda_{\text{int}} \rightarrow \infty$ and $m_\pi \rightarrow 0$, using the least squares fit. As shown in Fig. 3, the analysis shows that the extrapolation method yields results for g_T^{u-d} and κ_T^{u+d} that are consistent with those obtained without intermediate cutoff refinement. The real problem, however, arises from the tensor quadrupole moment Q_T^{u-d} . Like the usual quadrupole observables (electric quadrupole moment, D term), it depends strongly on

the pion Yukawa tail, which implies that the strong enhancement is expected at the small pion mass. However, the allowed pion mass when introducing the intermediate cutoff is about $m_\pi \geq 100$ MeV. This means that this method does not reflect the correct behavior of the tensor moments at the small pion mass and introduces huge uncertainties, especially for Q_T^{u-d} . Indeed, in Fig. 3 we observe that the results with the extrapolation underestimate the unrefined results, implying a loss of the chiral dynamics at small m_π . Therefore, we prefer the unrefined results in terms of chiral dynamics. However, this procedure remains important for the study of parton distribution functions.

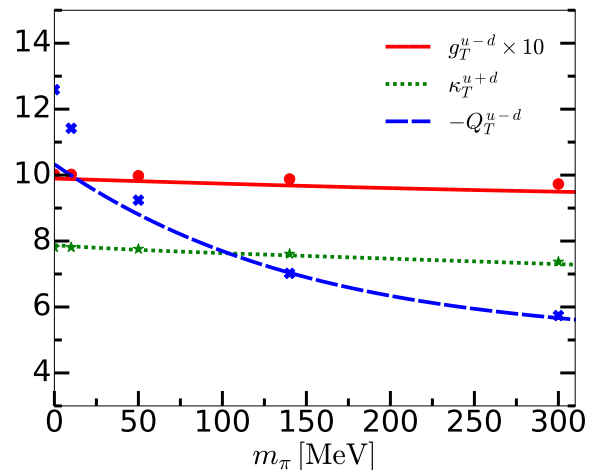


FIG. 3. Tensor multipole moments as a function of the pion mass: Extrapolated values to $\Lambda_{\text{int}} \rightarrow \infty$ and $m_\pi \rightarrow 0$ are compared with the unrefined ones. Circles (\bullet), stars (\star), and crosses (\times) denote the values of the tensor charge, anomalous tensor magnetic moment, and tensor quadrupole moment, respectively (unrefined method). Solid, dotted, and dashed curves depict the corresponding extrapolated functions (refined method).

-
- [1] X.-D. Ji, J. Phys. G **24**, 1181 (1998), arXiv:hep-ph/9807358.
- [2] K. Goeke, M. V. Polyakov, and M. Vanderhaeghen, Prog. Part. Nucl. Phys. **47**, 401 (2001), arXiv:hep-ph/0106012.
- [3] M. Diehl, Phys. Rept. **388**, 41 (2003), arXiv:hep-ph/0307382.
- [4] A. V. Belitsky and A. V. Radyushkin, Phys. Rept. **418**, 1 (2005), arXiv:hep-ph/0504030.
- [5] S. Boffi and B. Pasquini, Riv. Nuovo Cim. **30**, 387 (2007), arXiv:0711.2625 [hep-ph].
- [6] M. Guidal, H. Moutarde, and M. Vanderhaeghen, Rept. Prog. Phys. **76**, 066202 (2013), arXiv:1303.6600 [hep-ph].
- [7] K. Kumericki, S. Liuti, and H. Moutarde, Eur. Phys. J. A **52**, 157 (2016), arXiv:1602.02763 [hep-ph].
- [8] N. d'Hose, S. Niccolai, and A. Rostomyan, Eur. Phys. J. A **52**, 151 (2016).
- [9] J. C. Collins and M. Diehl, Phys. Rev. D **61**, 114015 (2000), arXiv:hep-ph/9907498.
- [10] D. Y. Ivanov, B. Pire, L. Szymanowski, and O. V. Teryaev, Phys. Lett. B **550**, 65 (2002), arXiv:hep-ph/0209300.
- [11] R. Enberg, B. Pire, and L. Szymanowski, Eur. Phys. J. C **47**, 87 (2006), arXiv:hep-ph/0601138.
- [12] B. Pire and L. Szymanowski, Phys. Rev. Lett. **103**, 072002 (2009), arXiv:0905.1258 [hep-ph].
- [13] M. El Beiyad, B. Pire, M. Segond, L. Szymanowski, and S. Wallon, Phys. Lett. B **688**, 154 (2010), arXiv:1001.4491 [hep-ph].
- [14] B. Pire and L. Szymanowski, Phys. Rev. Lett. **115**, 092001 (2015), arXiv:1505.00917 [hep-ph].
- [15] B. Pire, L. Szymanowski, and J. Wagner, Phys. Rev. D **95**, 094001 (2017), arXiv:1702.00316 [hep-ph].
- [16] G. Duplancić, S. Nabeebaccus, K. Passek-Kumerički, B. Pire, L. Szymanowski, and S. Wallon, Phys. Rev. D **107**, 094023 (2023), arXiv:2302.12026 [hep-ph].
- [17] S. Ahmad, G. R. Goldstein, and S. Liuti, Phys. Rev. D **79**, 054014 (2009), arXiv:0805.3568 [hep-ph].
- [18] S. V. Goloskokov and P. Kroll, Eur. Phys. J. C **65**, 137 (2010), arXiv:0906.0460 [hep-ph].
- [19] S. V. Goloskokov and P. Kroll, Eur. Phys. J. A **47**, 112 (2011), arXiv:1106.4897 [hep-ph].
- [20] S. V. Goloskokov and P. Kroll, Eur. Phys. J. C **74**, 2725 (2014), arXiv:1310.1472 [hep-ph].
- [21] B. Pasquini, M. Pincetti, and S. Boffi, Phys. Rev. D **72**, 094029 (2005), arXiv:hep-ph/0510376.
- [22] M. Burkardt and B. Hannafious, Phys. Lett. B **658**, 130 (2008), arXiv:0705.1573 [hep-ph].
- [23] C. Lorce, Phys. Rev. D **79**, 074027 (2009), arXiv:0708.4168 [hep-ph].
- [24] D. Chakrabarti, R. Manohar, and A. Mukherjee, Phys. Rev. D **79**, 034006 (2009), arXiv:0811.0521 [hep-ph].
- [25] N. Kumar and H. Dahiya, Phys. Rev. D **91**, 114031 (2015), arXiv:1506.03168 [hep-ph].
- [26] D. Chakrabarti and C. Mondal, Phys. Rev. D **92**, 074012 (2015), arXiv:1509.00598 [hep-ph].
- [27] K. Tezgin, B. Maynard, and P. Schweitzer, (2024), arXiv:2404.11563 [hep-ph].
- [28] M. Diehl and P. Hagler, Eur. Phys. J. C **44**, 87 (2005), arXiv:hep-ph/0504175.
- [29] J. P. Ralston and D. E. Soper, Nucl. Phys. B **152**, 109 (1979).
- [30] R. L. Jaffe and X.-D. Ji, Nucl. Phys. B **375**, 527 (1992).
- [31] R. L. Jaffe and X.-D. Ji, Phys. Rev. Lett. **67**, 552 (1991).

- [32] J. C. Collins, Nucl. Phys. B **394**, 169 (1993), arXiv:hep-ph/9207265.
- [33] V. Barone *et al.* (PAX), (2005), arXiv:hep-ex/0505054.
- [34] M. Anselmino, M. Boglione, U. D'Alesio, A. Kotzinian, F. Murgia, A. Prokudin, and C. Turk, Phys. Rev. D **75**, 054032 (2007), arXiv:hep-ph/0701006.
- [35] M. Anselmino, M. Boglione, U. D'Alesio, A. Kotzinian, F. Murgia, A. Prokudin, and S. Melis, Nucl. Phys. B Proc. Suppl. **191**, 98 (2009), arXiv:0812.4366 [hep-ph].
- [36] A. Bacchetta, A. Courtoy, and M. Radici, JHEP **03**, 119 (2013), arXiv:1212.3568 [hep-ph].
- [37] M. Anselmino, M. Boglione, U. D'Alesio, S. Melis, F. Murgia, and A. Prokudin, Phys. Rev. D **87**, 094019 (2013), arXiv:1303.3822 [hep-ph].
- [38] Z.-B. Kang, A. Prokudin, P. Sun, and F. Yuan, Phys. Rev. D **91**, 071501 (2015), arXiv:1410.4877 [hep-ph].
- [39] M. Göckeler, P. Hägler, R. Horsley, Y. Nakamura, D. Pleiter, P. E. L. Rakow, A. Schäfer, G. Schierholz, H. Stüben, and J. M. Zanotti (QCDSF, UKQCD), Phys. Rev. Lett. **98**, 222001 (2007), arXiv:hep-lat/0612032.
- [40] S. Park, R. Gupta, B. Yoon, S. Mondal, T. Bhattacharya, Y.-C. Jang, B. Joó, and F. Winter (Nucleon Matrix Elements (NME)), Phys. Rev. D **105**, 054505 (2022), arXiv:2103.05599 [hep-lat].
- [41] C. Alexandrou, M. Constantinou, K. Hadjiyiannakou, K. Jansen, and F. Manigrasso, Phys. Rev. D **104**, 054503 (2021), arXiv:2106.16065 [hep-lat].
- [42] T. Schäfer and E. V. Shuryak, Rev. Mod. Phys. **70**, 323 (1998), arXiv:hep-ph/9610451.
- [43] D. Diakonov, Prog. Part. Nucl. Phys. **51**, 173 (2003), arXiv:hep-ph/0212026.
- [44] D. Diakonov, V. Y. Petrov, and P. V. Pobylitsa, Nucl. Phys. B **306**, 809 (1988).
- [45] E. Witten, Nucl. Phys. B **160**, 57 (1979).
- [46] I. Zahed and G. E. Brown, Phys. Rept. **142**, 1 (1986).
- [47] M. Praszalowicz, A. Blotz, and K. Goeke, Phys. Lett. B **354**, 415 (1995), arXiv:hep-ph/9505328.
- [48] M. Praszalowicz, T. Watabe, and K. Goeke, Nucl. Phys. A **647**, 49 (1999), arXiv:hep-ph/9806431.
- [49] C. V. Christov, A. Blotz, H.-C. Kim, P. Pobylitsa, T. Watabe, T. Meissner, E. Ruiz Arriola, and K. Goeke, Prog. Part. Nucl. Phys. **37**, 91 (1996), arXiv:hep-ph/9604441.
- [50] J.-Y. Kim and C. Weiss, (2024), arXiv:2411.17634 [hep-ph].
- [51] H.-C. Kim, M. V. Polyakov, and K. Goeke, Phys. Rev. D **53**, 4715 (1996), arXiv:hep-ph/9509283.
- [52] H.-C. Kim, M. V. Polyakov, and K. Goeke, Phys. Lett. B **387**, 577 (1996), arXiv:hep-ph/9604442.
- [53] T. Ledwig, A. Silva, and H.-C. Kim, Phys. Rev. D **82**, 054014 (2010), arXiv:1007.1355 [hep-ph].
- [54] M. Diehl, Eur. Phys. J. C **19**, 485 (2001), arXiv:hep-ph/0101335.
- [55] P. Hagler, Phys. Lett. B **594**, 164 (2004), arXiv:hep-ph/0404138.
- [56] J.-Y. Kim, B.-D. Sun, D. Fu, and H.-C. Kim, Phys. Rev. D **107**, 054007 (2023), arXiv:2208.01240 [hep-ph].
- [57] D. Diakonov, M. V. Polyakov, and C. Weiss, Nucl. Phys. B **461**, 539 (1996), arXiv:hep-ph/9510232.
- [58] W. Pauli and S. M. Dancoff, Phys. Rev. **62**, 85 (1942).
- [59] S. Kahana, G. Ripka, and V. Soni, Nucl. Phys. A **415**, 351 (1984).
- [60] S. Kahana and G. Ripka, Nucl. Phys. A **429**, 462 (1984).
- [61] D. Diakonov, in *Advanced Summer School on Non-perturbative Quantum Field Physics* (1997) pp. 1–55, arXiv:hep-ph/9802298.
- [62] J.-Y. Kim, H.-Y. Won, J. L. Goity, and C. Weiss, Phys. Lett. B **844**, 138083 (2023), arXiv:2304.08575 [hep-ph].
- [63] P. Schweitzer, S. Boffi, and M. Radici, Phys. Rev. D **66**, 114004 (2002), arXiv:hep-ph/0207230.
- [64] P. Schweitzer, M. Colli, and S. Boffi, Phys. Rev. D **67**, 114022 (2003), arXiv:hep-ph/0303166.
- [65] M. P. Mattis, Phys. Rev. D **39**, 994 (1989).
- [66] M. P. Mattis and M. Mukherjee, Phys. Rev. Lett. **61**, 1344 (1988).
- [67] R. F. Lebed, Phys. Lett. B **639**, 68 (2006), arXiv:hep-ph/0603150.
- [68] G. S. Adkins, C. R. Nappi, and E. Witten, Nucl. Phys. B **228**, 552 (1983).
- [69] D. Diakonov, V. Petrov, P. Pobylitsa, M. V. Polyakov, and C. Weiss, Nucl. Phys. B **480**, 341 (1996), arXiv:hep-ph/9606314.
- [70] L.-H. Chan, Phys. Rev. Lett. **57**, 1199 (1986).
- [71] K. Goeke, J. Grabis, J. Ossmann, M. V. Polyakov, P. Schweitzer, A. Silva, and D. Urbano, Phys. Rev. D **75**, 094021 (2007), arXiv:hep-ph/0702030.
- [72] H. Alharazin, D. Djukanovic, J. Gegelia, and M. V. Polyakov, Phys. Rev. D **102**, 076023 (2020), arXiv:2006.05890 [hep-ph].
- [73] K. Goeke, J. Ossmann, P. Schweitzer, and A. Silva, Eur. Phys. J. A **27**, 77 (2006), arXiv:hep-lat/0505010.
- [74] I. A. Perevalova, M. V. Polyakov, and P. Schweitzer, Phys. Rev. D **94**, 054024 (2016), arXiv:1607.07008 [hep-ph].
- [75] M. V. Polyakov and P. Schweitzer, PoS **SPIN2018**, 066 (2019), arXiv:1812.06143 [hep-ph].
- [76] P. Schweitzer, D. Urbano, M. V. Polyakov, C. Weiss, P. V. Pobylitsa, and K. Goeke, Phys. Rev. D **64**, 034013 (2001), arXiv:hep-ph/0101300.
- [77] V. Pascalutsa, M. Vanderhaeghen, and S. N. Yang, Phys. Rept. **437**, 125 (2007), arXiv:hep-ph/0609004.
- [78] V. D. Burkert, L. Elouadrhiri, and F. X. Girod, Nature **557**, 396 (2018).
- [79] C. Alexandrou, K. Cichy, M. Constantinou, K. Hadjiyiannakou, K. Jansen, A. Scapellato, and F. Steffens, Phys. Rev. D **105**, 034501 (2022), arXiv:2108.10789 [hep-lat].
- [80] S. Kaur, S. Xu, C. Mondal, X. Zhao, and J. P. Vary (BLFQ), Phys. Rev. D **109**, 014015 (2024), arXiv:2307.09869 [hep-ph].
- [81] J. Kodaira, S. Matsuda, K. Sasaki, and T. Uematsu, Nucl. Phys. B **159**, 99 (1979).
- [82] X. Artru and M. Mekhfi, Z. Phys. C **45**, 669 (1990).
- [83] V. Barone, A. Drago, and P. G. Ratcliffe, Phys. Rept. **359**, 1 (2002), arXiv:hep-ph/0104283.
- [84] A. N. Manashov, S. Moch, and L. A. Shumilov, JHEP **09**, 192 (2024), arXiv:2407.12696 [hep-th].
- [85] J.-Y. Kim, Phys. Rev. D **108**, 034024 (2023), arXiv:2305.12714 [hep-ph].